Environmental Chemistry Letters (2018) 16:1393–1413
https://doi.org/10.1007/s10311-018-0768-x

REVIEW

Cyclodextrin-based supramolecular assemblies: a versatile toolbox for the preparation of functional porous materials

Rudina Bleta[1] · **Anne Ponchel**[1] · **Eric Monflier**[1]

Received: 13 June 2018 / Accepted: 20 June 2018 / Published online: 27 June 2018

Abstract
The discovery of ordered mesoporous materials in 1992 by Mobil Oil Corporation scientists has opened great opportunities for new applications in many emerging fields such as heterogeneous catalysis, biocatalysis, energy conversion, biosensors, photocatalytic devices and environmental technologies. Porous materials are grouped by the International Union of Pure and Applied Chemistry (IUPAC) into three classes according to their pore diameter: microporous (< 2 nm), mesoporous (2–50 nm) and macroporous (> 50 nm). One of the most versatile methods for the preparation of those materials is the soft template approach which combines the sol–gel process with molecular self-assembly. While the micelles formed by ionic or nonionic surfactants, as well as amphiphilic polymers, have been extensively used as templates, the supramolecular assemblies formed between cyclodextrins and block copolymers have been less investigated, despite their large chemical and structural diversity. This review article focuses mainly on nanostructured porous inorganic materials derived from cyclodextrins or cyclodextrin-based assemblies. More than 100 references are described and discussed, in which we look both at their synthesis and characterization, as well as their applications in the emerging fields of heterogeneous catalysis and photocatalysis. A special attention is paid to the evaluation of the critical parameters that need to be controlled for improving their (photo) catalytic performances.

Keywords Colloids · Sol–gel · Porous materials · Cyclodextrins · Template · Nanocasting · Heterogeneous catalysis · Photocatalysis

Introduction

Nanostructured porous materials have attracted tremendous research interest during the past two decades due to their unique structural and functional properties (Davis 2002; Lu and Schüth 2006; Imhof and Pine 1997; Velev and Kaler 2000). As reported in a large number of well-documented reviews, these materials offer potential applications in many emerging fields such as heterogeneous catalysis, energy conversion and storage devices, electrochemistry, optics, membranes and separation, drug delivery, biocatalysis, biosensors, photocatalytic devices and environmental technologies (Corma 1997; Walcarius 2013; Zhu et al. 2015; Sun et al. 2016). Although a wide range of synthesis and assembly strategies have been developed so far for the fabrication of materials with tunable properties, the template synthesis remains one of the most flexible and important approaches to generate self-assembled nanostructures with well-defined architectures and hierarchical order at multiple length scales (Liu et al. 2013; Velev and Kaler 2000; Yang et al. 2017; Blin et al. 2006; Bleta et al. 2006). As both the structure and the composition of the template play a crucial role in the properties of the resulting material, there is a need to develop new supramolecular templates with tailored properties. In this context, cyclodextrins are of special interest owing to their unusual structural polymorphism as well as their ability to generate, in association with polymers, a wide range of fascinating architectures (Szejtli 1998; Breslow and Dong 1998; Wenz 1994; Born and Ritter 1995; Harada 1996, 2001; Herrmann et al. 1997).

In this review article, we aim to highlight the recent developments on the use of the native and modified cyclodextrins, as well as the supramolecular assemblies that they form by host–guest interactions with polymers, as excellent

✉ Rudina Bleta
rudina.bleta@univ-artois.fr

[1] Univ. Artois, CNRS, Centrale Lille, ENSCL, Univ. Lille, UMR 8181, Unité de Catalyse et Chimie du Solide (UCCS), 62300 Lens, France

candidates for fabricating functional inorganic materials with precise control over the pore size and structure, the particle shape, the crystal phase composition and the spatial arrangement of nanoparticles. The three main topics that we aim to highlight are: (1) the use of nanocasting as a flexible and versatile strategy for replicating the architecture of cyclodextrin-based aggregates, poly*pseudo*rotaxanes and three-dimensional hydrogels to create hierarchically structured porous silica materials with well-defined spatial arrangement of the mico-, meso- and macropores, (2) elaboration of nanostructured metal oxide materials, other than silica, by template-directed colloidal self-assembly using cyclodextrin-based supramolecular assemblies as soft template and sol–gel synthesized colloidal particles as building blocks; (3) some applications of these materials in the emerging fields of heterogeneous catalysis and photocatalytic degradation of pesticides from wastewater.

This review article is an abridged version of the chapter published by Bleta et al. (2018a, b) in the series Environmental Chemistry for a Sustainable World (https://www.springer.com/series/11480).

Main strategies toward the synthesis of nanostructured silica materials

Natural porous materials and biomimetic design

Porous materials occur widely in nature. Diatoms and radiolarians are most famous examples of natural porous materials living in most aquatic environments and using photosynthesis as a source of energy. One of the most remarkable features of these unicellular microalgae is their cell wall which is build up of a silicified shell, also known as the frustule. The diatom frustule displays a highly porous hierarchical structure and exhibits an extremely high mechanical stability which can be retained over geological timescales (Kooistra et al. 2007; Hildebrand 2008). Moreover, diatoms also play a major role in the carbon cycle of our Earth since they produce through photosynthesis about one-fifth of the oxygen we breathe (Kröger and Poulsen 2008). They act therefore as major contributors to global carbon dioxide fixation (Armbrust et al. 2004; Armbrust 2009).

The diatom frustule is partly organic (proteins and polysaccharides) and partly bioinorganic (hydrated silicon, $SiO_2 \cdot [H_2O]_n$) and is formed through a remarkably rapid biomineralization process that is accomplished under mild physiological condition (Sumper et al. 2007; Kröger et al. 1999). The frustule presents a well-defined hierarchical structure where several nanoscale elements (pores, channels) are regularly arranged in a complex 3D architecture with high level of precision. This porous structure is incredibly robust and confers to diatoms remarkable properties, such as mechanical strength, density, permeability, color and hydrophobicity (Hamm et al. 2003). Silaffin polypeptides were found to play a crucial role in the self-assembly process which guides the formation of the silica network. Therefore, the understanding of the mechanism of fabrication of the diatom frustule is essential for developing new synthetic routes toward novel nanostructured materials that mimic natural systems.

The concept of nanocasting

Over the past 25 years, since the discovery of mesoporous materials by the group of Mobil Oil Corporation (Kresge et al. 1992; Beck et al. 1992), many research groups have proposed different biomimetic approaches to build materials with multiscale porous structures, similar to those of diatoms. One of the most well-known approaches is the nanocasting route which has proved to be straightforward for the synthesis of a wide range of nanostructures from a template (Wan and Zhao 2007). Generally, two kinds of templates, defined as hard- and soft templates, are described in the literature. Hard templates are solid-state materials with particular structure and morphology, such as mesoporous silica, usually used for the synthesis of ordered carbon materials. On the other hand, soft templates are usually in a fluid-like state and have attracted attention, especially for the synthesis of mesoporous inorganic materials with tailorable pore structures.

Various supramolecular assemblies prepared from ionic or nonionic surfactants or water-soluble polymers can be used as soft templates to prepare well-ordered mesoporous silica with monodisperse pore sizes (Lu and Schüth 2006). Most common mesoporous silicas are the small pore hexagonal Mobil Composition of Matter-41 (MCM-41), cubic MCM-48, lamellar MCM-50, the large pore hexagonal Santa Barbara Amorphous-15 (SBA-15) and cubic SBA-16, as well as Hexagonal Mesoporous Silica (HMS) and Michigan State University (MSU) materials with wormlike pore structure (Fig. 1).

Most of them are prepared quite easily, under mild conditions, using the sol–gel process. The sol–gel synthesis involves the hydrolysis and catalytic polycondensation of a silicon alkoxide precursor (e.g., tetramethoxysilane or tetraethoxysilane) in the presence of a supramolecular template (typically micelles formed by amphiphilic molecules). The macromolecular network of siloxane bonds can be obtained by two different ways, i.e., via a cooperative assembly process taking place in situ between the structure directing agent and the silica precursor in solution, or through a true liquid–crystal-phase templating (TLCT) mechanism, by the formation of a silica framework around the preformed liquid crystal mesophase (Fig. 2).

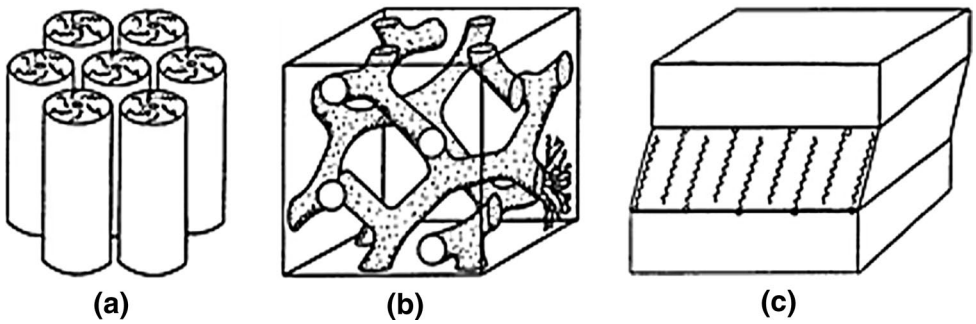

Fig. 1 Different types of mesoporous materials. **a** Hexagonal arrangement of pores: type Mobil Composition of Matter-41 (MCM-41); **b** cubic arrangement of pores: type MCM-48; **c** Lamellar arrangement of pores: type MCM-50. Reprinted with permission of the Royal Society of Chemistry from Corma et al. (2008)

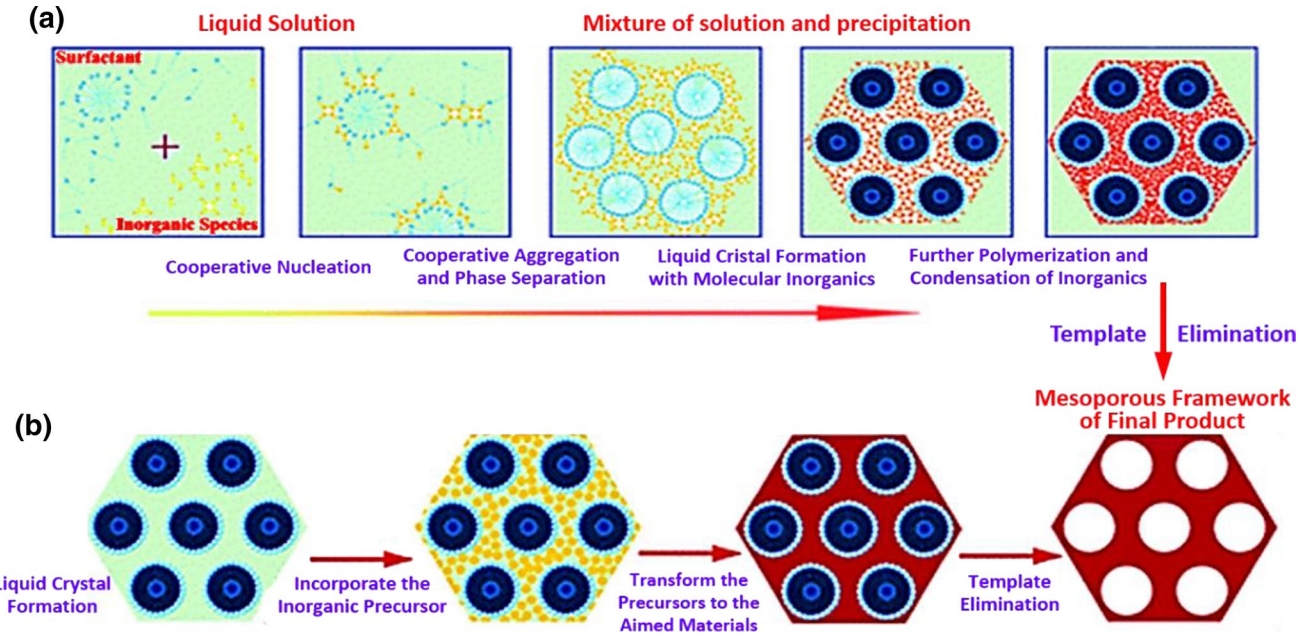

Fig. 2 Schematic representation of the soft-templating method via two synthetic strategies: **a** cooperative self-assembly and **b** "true liquid–crystal templating" (TLCT) process for the synthesis of ordered mesoporous materials. Reprinted with permission from Wan and Zhao (2007). Copyright 2007 American Chemical Society

It is worth emphasizing that the cooperative assembly process is not a nanocasting route since it does not replicate a preformed surfactant structure. For instance, in the synthesis of mesoporous silica, concentrations of surfactant even below the critical micelle concentration (CMC) can yield highly ordered mesoporous structures. These materials are usually highly porous (pore volume higher than 0.7 $cm^3\ g^{-1}$), possess large surface areas (up to 1500 $m^2\ g^{-1}$), well-defined multiscale porous networks, tunable pore sizes and interconnectivity. These properties make them viable for applications in different emerging fields ranging from biotechnology, biomedicine, drug delivery, catalysis, energy storage, optics, separation processes to immobilization of biomolecules and bio-organisms as well as bone regeneration (Su et al. 2012).

Using cyclodextrin-based supramolecular assemblies as templates

The structure and properties of the template play a crucial role with respect to the properties of the replicated porous material. In this context, cyclodextrins (CDs) offer attractive alternative to surfactants owing to the rich structural diversity of the supramolecular assemblies that they form in aqueous phase in association with polymers. Cyclodextrins are water-soluble cyclic oligosaccharides composed of a hydrophobic internal cavity and a hydrophilic exterior surface due to the presence of a large number of hydroxyl groups. Most common cyclodextrins contain six (α-CD), seven (β-CD) and eight (γ-CD) glucopyranose units in the ring (Fig. 3). These molecules demonstrate

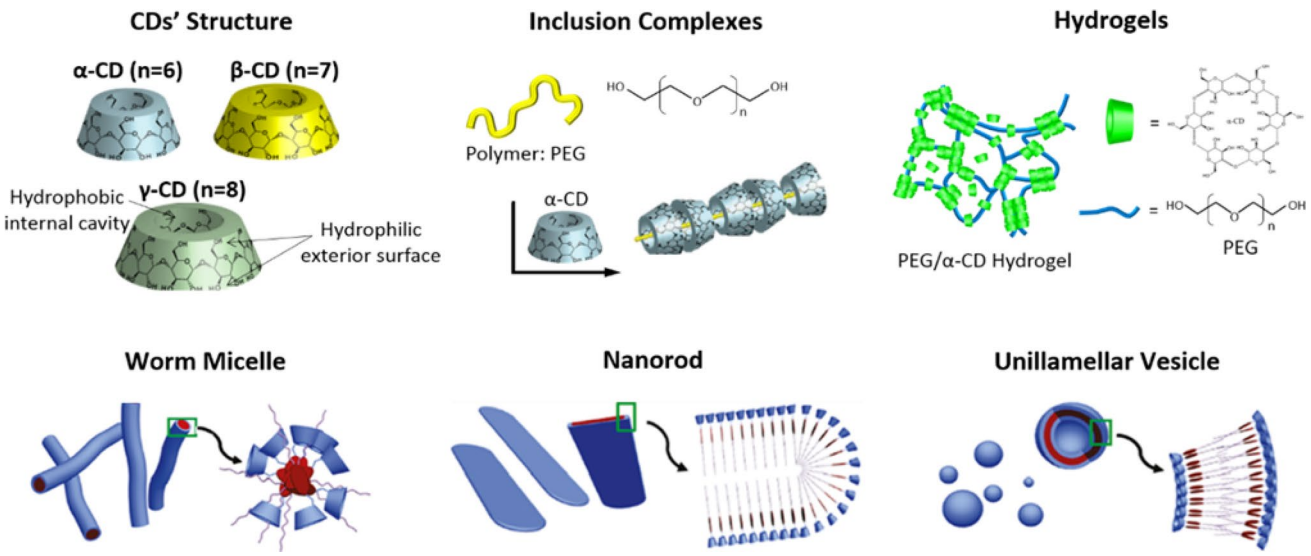

Fig. 3 Cyclodextrins (CD) structure and cyclodextrin-based nanosystems formed by their self-assembly with polymers. Adapted with permission from Harada et al. (2009) and Jiang et al. (2010). PEG: poly(ethylene glycol) Copyright 2009 and 2010 American Chemical Society

multifunctional properties, such as the ability to form supramolecular assemblies with a large variety of intriguing structures with amphiphilic surfactants of appropriate size and shape (Szejtli 1998; Breslow and Dong 1998; Wenz 1994; Born and Ritter 1995; Harada 1996, 2001; Herrmann et al. 1997; Fig. 3). Since the pioneering works of Harada and Kamachi (1990), who showed that α-CD can form inclusion complexes with poly(ethylene glycol) (PEG) in aqueous solution to give poly*pseudo*rotaxanes with a necklace-like structure, a range of polymeric guests have been investigated (Harada et al. 2009). A particular attention has been paid to the interactions occurring between the native β-CD and nonionic triblock copolymers of the poly(ethylene oxide) (PEO)-*b*-poly(propylene oxide) (PPO)-*b*-poly(ethylene oxide) (PEO) family, also known as Pluronics. Thus, it has been shown that the native β-CD can slide along the hydrophilic extremity PEO blocks of the Pluronic P84 ($PEO_{19}PPO_{43}PEO_{19}$) to selectively thread the middle hydrophobic PPO blocks and form poly*pseudo*rotaxanes with a well-ordered channel structure.

Despite their rich structural polymorphism, the supramolecular assemblies formed between block copolymers and CD-derivatives have been very little used as soft templates. In the field of materials science, micelles and lyotropic phases are the most commonly used templates for the synthesis of porous materials with controlled architectures. On the other hand, the possibility of using CDs or CD/polymer assemblies as supramolecular templates has been reported only in few studies and most of them have been devoted to the synthesis of mesoporous silica by sol–gel process (Polarz et al. 2001; Han and Antonietti 2002; Han et al. 2003).

Microporous silica from cyclodextrins

The possibility to extend the principle of nanocasting from micelles and lyotropic phases to cyclodextrins was first demonstrated by Antonietti et al. (Polarz et al. 2001; Polarz and Antonietti 2002; Antonietti 2006) who employed the aggregates formed by native and modified cyclodextrins in water as templates in the nanocasting process. Cyclodextrins have the ability to self-assemble in water into assemblies with a "molecular barrel" structure (Saenger 1980). These "barrels" have an exterior surface covered by –OH groups, while the interior cavity is quite hydrophobic, characterized by exposure of $–CH_2–$ groups. Owing to the rich OH-functionality on their outside surface, cyclodextrin assemblies in water can be nanocasted. Interestingly, the silica materials prepared by nanocasting were "worm-type" and presented a very similar structure to those obtained with classical amphiphiles (Fig. 4). The pore size corresponded exactly to the diameter of the cyclodextrin, while the length was significantly larger. The pore cross section of these materials, as determined by porosimetry, was nicely correlated with the molecular diameter of the cyclodextrins. Thus, using the hydroxypropylated α-CD (HPα-CD) assemblies, 1.4 nm pores were obtained, while the replication of the HPγ-CD assemblies led to 1.8 nm pores. Such a direct correlation is an important indication that the pore systems result really from the "molecular barrel" structure of the CD assemblies. The difference between the hydrophilic exterior and the hydrophobic interior of the CD-molecule was supposed to be the driving force for this assembly.

This result was particularly interesting since it showed for the first time that, besides offering the possibility to

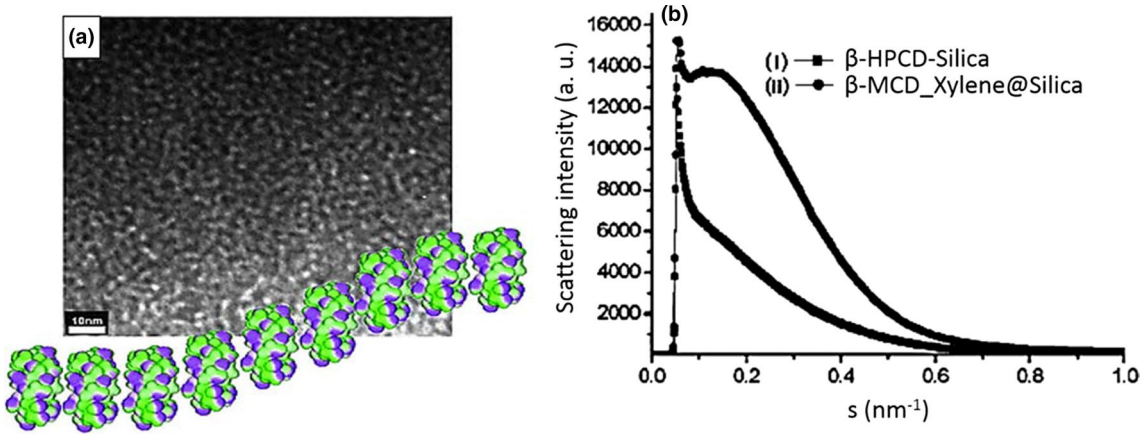

Fig. 4 **a** Transmission electron microscopy (TEM) image of a representative cyclodextrin (CD)-based silica demonstrating the "worm-type" architecture of the pores and a schematic image of the CD-alignment indicating the template structure; **b** small-angle X-ray scattering (SAXS) diffractograms of two CD-based porous materials: (i) one was prepared using the hydrophilic hydroxypropylated β-CD (β-HPCD) showing a rather disordered pore-system, (ii) the other one was prepared with the more hydrophobic xylene@methylated β-CD (β-MCD) possessing strong quadrupolar amphiphilic character. The latter pore-system is much more ordered and uniform. Reprinted with permission of the Royal Society of Chemistry from Polarz and Antonietti (2002)

synthesize nanostructured silica materials, nanocasting can also be used as "analytical tool" to examine the soft and delicate structure of these assemblies. Thus, instead of investigating the soft-matter structure in its dispersion medium itself, it is possible to examine its "hardcopy" derived by nanocasting. This route has several potential advantages in comparison with the direct examination of the organic template due to the higher electron contrast and higher stability of the solid matter against most experimental conditions, such as electron microscopy or scattering techniques.

Mesoporous silica from cyclodextrin-based poly*pseudo*rotaxanes

Besides cyclodextrins, poly*pseudo*rotaxanes can also be replicated into mesoporous silica (Han and Antonietti 2002). It has been reported that in the case of triblock copolymers, the native α-CD preferentially binds the PEO units, whereas the native β-CD slides along the hydrophilic extremity PEO blocks to selectively thread the middle hydrophobic PPO blocks (Harada 1996; Harada et al. 2009). The resulting poly*pseudo*rotaxanes present a "string-of-pearl" morphologies. Remarkably, these poly*pseudo*rotaxanes were shown to spontaneously self-assemble in water to generate other types of supramolecular assemblies with a well-defined crystalline structure. Thus, by using small-angle neutron scattering (SANS) and atomic force microscopy (AFM), it was demonstrated that the self-assembly of β-CD and Pluronic F68 ($PEO_{80}PPO_{27}PEO_{80}$) micelles gives cylindrical bundles, which can then act as building blocks for the formation of flat and rigid platelets with well-defined angles at 40 °C (Travelet et al. 2008, 2009, 2010). When these in situ formed supramolecular assemblies were used as templates for the synthesis of silica materials, a pH-dependent behavior was noticed on the pore diameter (Han and Antonietti 2002). Direct replication was obtained at pH 2, whereas larger pores were formed at pH values between 3 and 4. As the structure of silica does not change strongly in the pH range between 2 and 4, the increase in the pore size was directly related to the aggregation of poly*pseudo*rotaxanes into arrays or bundle structures that can generate larger pores by nanocasting. Later, the nanocasting was also extended to stable isolated poly*pseudo*rotaxanes obtained from α-CD and polyamines (Han et al. 2003). The resulting silica materials possessed an approximate replica of the original rod-like rotaxanes with a homogeneous distribution of the pores.

Hierarchically porous silica from polyethylene glycol/α-cyclodextrin hydrogels

Not only cyclodextrin barrels or poly*pseudo*rotaxanes, but also highly reticulated hydrogels and their self-assembly motifs, can be replicated. Thus, the silicification by sol–gel process of the polyethylene glycol/α-cyclodextrin (PEG/α-CD) hydrogels yielded nanostructured silica materials with bimodal or trimodal pore size distributions (Fig. 5; Bleta et al. 2014c).

Hydrogels can be defined as water-swollen hydrophilic polymers, formed by covalent bonds or physical cohesion forces between the polymer segments, such as van der Waals forces, hydrophobic interactions or hydrogen bonds. The pioneering work of Li et al. (1994) showed that the native α-CD and a high molecular weight PEG (higher than 10,000 g mol^{-1}) can spontaneously form a three-dimensional

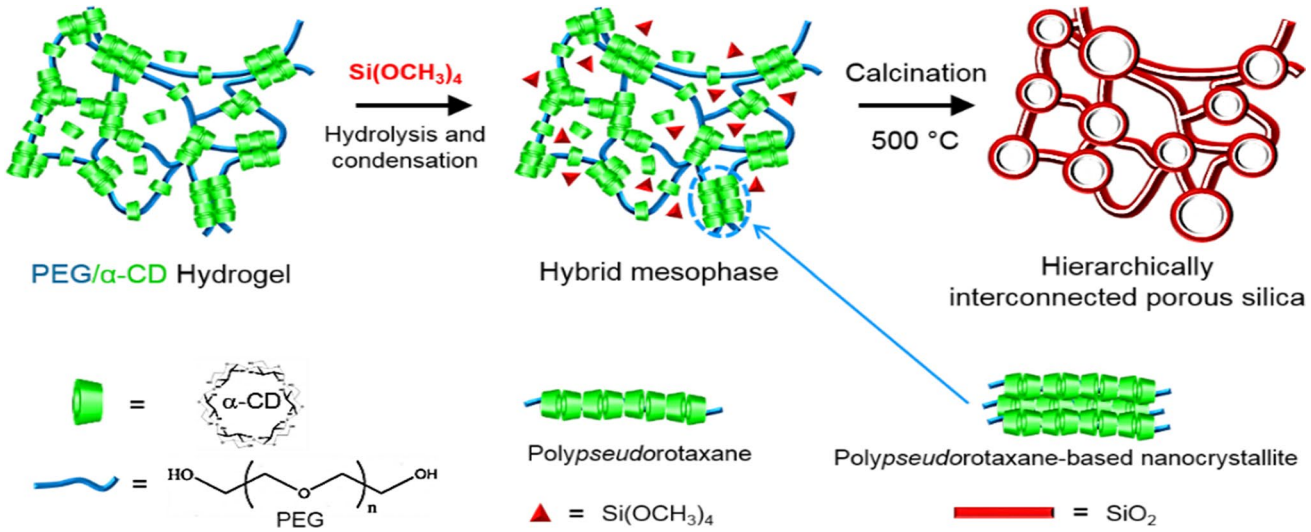

Fig. 5 Schematic illustration of the template-directed synthesis of silica materials with hierarchical pore architectures where the large mesopores are interconnected by small mesopores in a three-dimensional framework. The cross-linking of these poly*pseudo*rotaxanes into columnar nanocrystallites with a channel-like architecture directs the condensation of silica in a bi- or trimodal porous network. PEG: poly(ethylene glycol) and α-CD: native α-cyclodextrin. Reprinted with permission of the Royal Society of Chemistry from Bleta et al. (2014c)

physically cross-linked hydrogel by host-gust interactions. A large amount of water can be entrapped within the macroscopic voids. Gelation was proposed to occur via the cross-linking of the partially formed PEG/α-CD inclusion complexes, which further self-assemble into water insoluble poly*pseudo*rotaxanes with a channel-like structure (Li et al. 1994). Subsequently, the individual poly*pseudo*rotaxanes further grow in size, aggregate and finally phase-separate. As stated by Weickenmeier and Wenz (1997), the phase-separation is followed by the threading of additional α-CD onto the polymer chains, leading to the aggregation and growth of columnar poly*pseudo*rotaxane-based nanocrystallites (Travelet et al. 2009, 2010). This nanoscale arrangement of poly*pseudo*rotaxanes into nanocrystallites is assumed to play a crucial role in maintaining the hydrogel in a water-swollen state.

To investigate in detail how the PEG concentration affects the gelation behavior, a series of silica materials were prepared by templating the hydrogels prepared in a saturated α-CD solution (100 mg mL^{-1}) at pH 4 and 2 with increasing amounts of PEG (1–30 mg mL^{-1}) (Bleta et al. 2014c). The chemistry of silica does not change significantly in this pH range, which is close to the isoelectric point of the silicic acid, where the condensation rate is the slowest. So, the variations monitored in the porosity of the materials can be mainly attributed to the structural changes occurring within the hydrogel template in response to pH.

The N_2-adsorption analyses of the silica materials prepared at pH 4 indicated the formation of a hierarchical pore structure with three types of pores: (1) micropores (1.8 nm) associated with naked polymer chains, (2) small mesopores (2.0, 2.3 nm) associated with individual poly*pseudo*rotaxanes, as well as (3) larger mesopores (5.8 nm) associated with the columnar α-CD crystallites formed by the self-assembly of poly*pseudo*rotaxanes at their CD-rich segments. Moreover, nanocrystallites were found to gradually grow in size as the solution was loaded with more PEG and as the hydrogel network became denser. On the other hand, all materials prepared at pH 2 contained a higher amount of micropores (1.8 nm) and small mesopores (2 nm), even at a high PEG concentration (30 mg mL^{-1}) indicating that, under more acidic conditions, more unthreaded α-CD and uncovered PEG segments are available, thus leading to lower cross-linking densities within the hydrogel network.

Representative electronic microscopy images (SEM and TEM) showed that the silicified hydrogels at pH 4 tended to form mica-like sheets assembled in a "gypsum flower" morphology (Fig. 6a) with long tubular structures (about 30–170 nm in diameter) made up of several linear strings associated with the bundles of poly*pseudo*rotaxanes (Fig. 6b). Moreover, from TEM observations, some local order was also noticed in the mesoporous network (Fig. 6c). Interestingly, the small-angle X-ray scattering (SAXS) data indicated the presence of two reflection peaks at $2\theta = 1.51°$ and 2.65° (q ratios $1:\sqrt{3}$), corresponding to d-spacing values of 5.84 nm and 3.33 nm, respectively, which can be indexed to the (100) and (110) Bragg reflections of a hexagonal mesostructured (Fig. 6d). This means that some local order exists within these silica replicas, due to the self-assembly of poly*pseudo*rotaxanes in rather regular columnar bundles

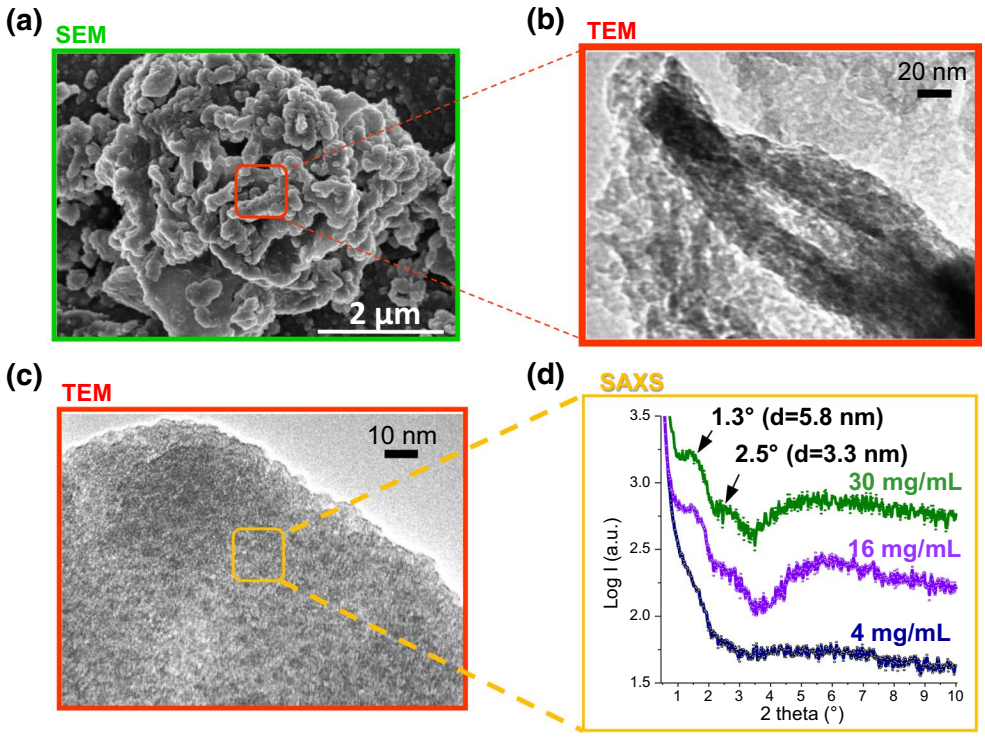

Fig. 6 Scanning (SEM) (**a**) and transmission electron microscopy (TEM) (**b**, **c**) images of the calcined silica materials prepared from poly(ethylene) glycol (PEG) (30 mg mL^{-1})/α-CD (100 mg mL^{-1}) hydrogels at pH 4. Note the presence of long tubular structures with 30–170 nm diameters associated with the bundles of poly*pseudo*rotaxanes. Small-angle X-ray scattering (SAXS) plots of silica materials prepared with increasing amounts of PEG (from 4 to 30 mg/mL) (**d**). All samples were calcined at 500 °C for 16 h. Adapted with permission of the Royal Society of Chemistry from Bleta et al. (2014c)

within the crystallites. On the other hand, sharper striations were formed in the hydrogel silicified at pH 2 where the mesoporous network was characterized by the presence of regular lattice fringes consistent with a higher degree of structuration.

Main strategies for the synthesis of non-siliceous mesoporous oxides

The template-directed colloidal self-assembly approach

Non-siliceous mesoporous metal oxides such as TiO_2 and Al_2O_3 are very difficult to prepare via a direct templating approach (i.e., using the cooperative self-assembly or the true liquid–crystal-phase templating (TLCT) processes, Fig. 2). Indeed, compared to silicon alkoxides, the hydrolysis and condensation of transition metal alkoxides are not easy to control precisely in aqueous phase. The resulting materials are generally not robust enough to maintain the mesostructure after the formation of the oxide framework, and they usually exhibit very poor crystallinity and low thermal stability after the template removal (Van Der Voort et al. 2008).

A versatile strategy to overcome the limitations of the cooperative self-assembly or the TLCT processes, and extend the scope of nanostructured porous materials beyond silica, is the so-called template-directed colloidal self-assembly approach (or the nanoparticle route) (Bleta et al. 2010). This approach involves the use of pre-synthesized colloidal particles that have the ability to self-assemble around a soft template (e.g., block copolymer or biopolymer). After drying and calcination, the recovered mesoporous materials are usually robust and present high surface areas, large pore volumes and tunable porosities (Bleta et al. 2010, 2012). Nanoparticles can be held together either by weak noncovalent forces, such as hydrogen bonding (Boal et al. 2000; Hao and Lian 2000) or by strong covalent bonds via different functional groups that can be fixed onto the nanoparticle surface (Patolsky et al. 2002; Lu et al. 2003). So far, the template-directed colloidal self-assembly has been successfully employed for the preparation of a variety of inorganic materials, especially semiconductor metal oxide nanoparticles, whose structural and textural characteristics depend on the characteristics of both the template and the colloidal nanocrystals (Yu and Peng 2002; Rajh et al. 1993). This

approach was successfully used also for the synthesis by sol–gel process of mesoporous γ-Al_2O_3 and TiO_2 materials from the supramolecular assemblies formed between cyclodextrins and block copolymers in water (Fig. 7).

Mesoporous non-siliceous oxides from RaMe*β*-CD/Pluronic P123 assemblies

Interactions between RaMe*β*-CD and Pluronic P123

Before using the cyclodextrin/polymer assemblies as template, it is necessary to study their interactions in aqueous phase. Since the pioneering works of Harada et al. (Harada and Kamachi 1990) who showed that *α*-CD can form inclusion complexes with poly(ethylene glycol) (PEG) in aqueous solution to give poly*pseudo*rotaxanes with a necklace-like structure, a wide range of polymeric guests have been reported to form inclusion complexes with cyclodextrins (Harada 1996). However, compared to the native CDs, the interactions between the modified CDs and polymers have been less investigated in the literature. The results reported by Gaitano et al. (1997), and later supported by other authors (Joseph et al. 2007; Lazzara and Milioto 2008; Nogueiras-Nieto et al. 2009; Dreiss et al. 2009; Tsai et al. 2010), showed that, similarly to the native *β*-CD, the macrocycle of a dimethylated *β*-CD is able to complex the hydrophobic poly(propylene oxide) blocks of different nonionic triblock copolymers of the poly(ethylene oxide) (PEO)-*b*-poly(propylene oxide) (PPO)-*b*-poly(ethylene oxide) (PEO) family (i.e., Pluronics). On the other hand, spectroscopic and time-resolved small-angle neutron scattering measurements performed on mixtures of heptakis (2,6-di-o-methyl)-*β*-CD and three Pluronics [P123 ($PEO_{20}PPO_{70}PEO_{20}$), P85 ($PEO_{39}PPO_{52}PEO_{39}$) and F127 ($PEO_{107}PPO_{70}PEO_{107}$)] evidenced that the micellar rupture occurs with extremely fast kinetics, thus excluding the possibility of poly*pseudo*rotaxane formation via inclusion complexation (Valero et al. 2012). Interestingly, in the case of Pluronic P123, the authors reported a possible restructuration of the micelles toward swollen lamella, with an interlayer spacing that was much higher than the typical values reported in the literature with conventional swelling agents (Holmqvist et al. 1998). However, the phenomenon of micellar rupture was shown to be highly sensitive to the substitution degree, nature and position of the modified groups within the cyclodextrin (Joseph et al. 2007; Valero et al. 2012). Thus, in contrast to the micellar rupture observed with the heptakis (2,6-di-o-methyl)-*β*-CD, micelles remained intact in the presence of other substituted β-cyclodextrin derivatives, such as the 2,3,6-trimethyl-*β*-CD, 2-hydroxyethyl-*β*-CD and 2-hydroxypropyl-*β*-CD (Valero et al. 2012).

We have investigated the supramolecular associations occurring between the block copolymer Pluronic P123 and the randomly methylated *β*-CD (RaMe*β*-CD) with the attempt to use these assemblies as templates for the synthesis of porous inorganic solids (Bleta et al. 2013, 2014b). Indeed, this cyclodextrin is highly soluble in water, cheap, non-toxic, commercially available (Uekama and Irie 1987) and surface active (Leclercq et al. 2007). The surface tension measurements indicated that the critical micelle concentration (CMC) of the copolymer was not significantly affected by the addition of RaMe*β*-CD whatever the molar ratio of RaMe*β*-CD to P123 used (in the range of 1.7–7.1), thus indicating that their interactions are relatively weak and do not affect significantly the micellization process. Indeed, if the hydrophobic interactions between the PPO chains, which are the driving force for the micellization, are screened by the presence of the cyclodextrin, this may lead to a disruption of the copolymer micelles and an increase of the CMC (Bernat et al. 2008; Mahata et al. 2010). Moreover, the size

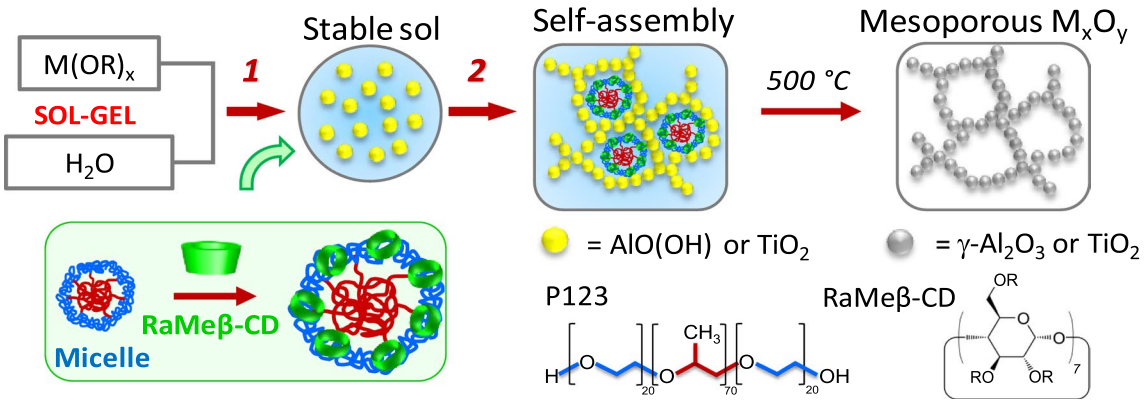

Fig. 7 Schematic illustration of the template-directed colloidal self-assembly approach where the colloidal nanoparticles act as building blocks for the construction of the inorganic network around the supramolecular template. Metal alkoxides $M(OR)_x$ (M: metal; R: alkyl group) are typically used as precursors for the synthesis of the colloidal solution (sol). Metal oxides (M_xO_y) are produced after calcination at 500°C. RaMe*β*-CD: Randomly Methylated *β*-CD and P123: Pluronic $PEO_{20}PPO_{70}PEO_{20}$

distribution plots, determined by dynamic light scattering (DLS) (Fig. 8), indicated a progressive increase in the hydrodynamic radius of Pluronic micelles with increasing the RaMe*β*-CD/P123 molar ratio (RaMe*β*-CD/P123 varying from 1.7 to 5.7). Such increase in the size of the micelles was attributed to the ability of the methylated cyclodextrin to act as a swelling agent by locating preferentially at the interface layer of the block copolymer micelles, in interaction with the hydrophobic PPO blocks. The scattering intensity of these assemblies gradually decreased with the RaMe*β*-CD concentration due to the formation of less well-defined objects with more flexible interfaces.

Mesoporous γ-Al_2O_3 materials with tunable porosity

Aluminum oxide and hydroxides have been the subject of intensive academic and industrial research over the past three decades (Misra 1986). In particular, mesoporous γ-alumina (γ-Al_2O_3) with crystalline framework, large pore volume and high surface area, which has also proven robustness and stability in water (Bleta et al. 2018b), is the ideal support for potential applications in automotive and petroleum industries (Misra 1986) as well as catalysis (Alphonse et al. 2015).

We employed the above RaMe*β*-CD/Pluronic P123 assemblies as soft templates to prepare mesoporous γ-Al_2O_3 materials with tunable porosity by using boehmite (AlO(OH)) colloids synthesized in aqueous solution (H_2O/Al ≈ 100) as building blocks (Bleta et al. 2011; Fig. 9a). The P123 concentration was fixed at 7.8% (PEO/Al = 1), whereas the RaMe*β*-CD concentration was varied from 30 to 130 mg mL^{-1} (i.e., RaMe*β*-CD/P123 molar ratio in the range of 1.7–7.1). After thermal treatment at 500 °C, the morphology of the resulting materials was fibber-like and several voids with an average diameter of ~ 20 nm were also noticed (see circles Fig. 9b), indicating that the material successfully adopted some characteristics of the supramolecular template. Moreover, a remarkable increase in the surface area (from 220 to 380 m^2/g), pore size (from 5.6 to 20 nm) and pore volume (from 0.3 to 2.0 cm^3/g) was noticed from the N_2-adsorption analysis (Fig. 9c, Table 1). Such improvement in both the structural and textural characteristics of γ-Al_2O_3 was directly related to the ability of RaMe*β*-CD to act as micelle expander and restructure the γ-Al_2O_3 particle network. XRD analysis also confirmed that the boehmite was successfully transformed into γ-Al_2O_3 after calcination at 500 °C (Fig. 9d). Hence, the void space formed between the nanoparticles may be seen as a solid replica of the original swollen micelles formed by the coassembly of the copolymer and the cyclodextrin.

Mesoporous TiO_2 from different cyclodextrins as structure directing agents

The template-directed colloidal self-assembly approach was successfully extended to mesoporous titanium dioxide (TiO_2) using both RaMe*β*-CD-swollen Pluronic micelles (Lannoy et al. 2014) and various cyclodextrins as structure directing agents (Bleta et al. 2014a). TiO_2 has been applied as one of the most promising photocatalysts for the removal of industrial organic pollutants from water and air (Zhao et al. 2004; Gomathi et al. 2013), as well as for the photocatalytic water splitting for hydrogen production (Fujishima and Honda 1972). TiO_2 commonly crystallizes in three polymorphic forms, i.e., anatase (tetragonal, I41/amd), brookite (orthorhombic, Pbca) and rutile (tetragonal,

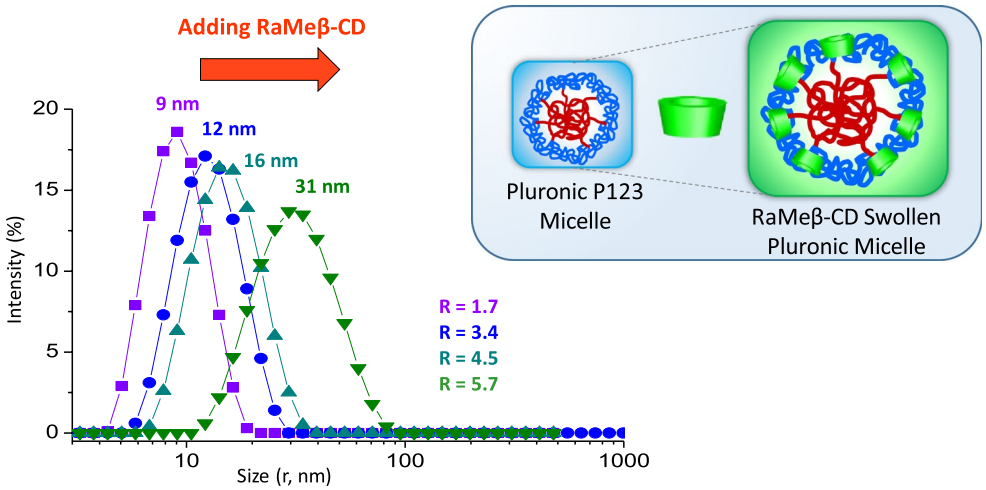

Fig. 8 Dynamic light scattering data (DLS) of Pluronic P123 ($PEO_{20}PPO_{70}PEO_{20}$) micellar solutions prepared with various amounts of Randomly Methylated *β*-CD (RaMe*β*-CD) (RaMe*β*-CD/P123 molar ratios from 1.7 to 5.7). All measurements were performed at 25 °C. Adapted with permission from Bleta et al. (2013). Copyright 2013 American Chemical Society

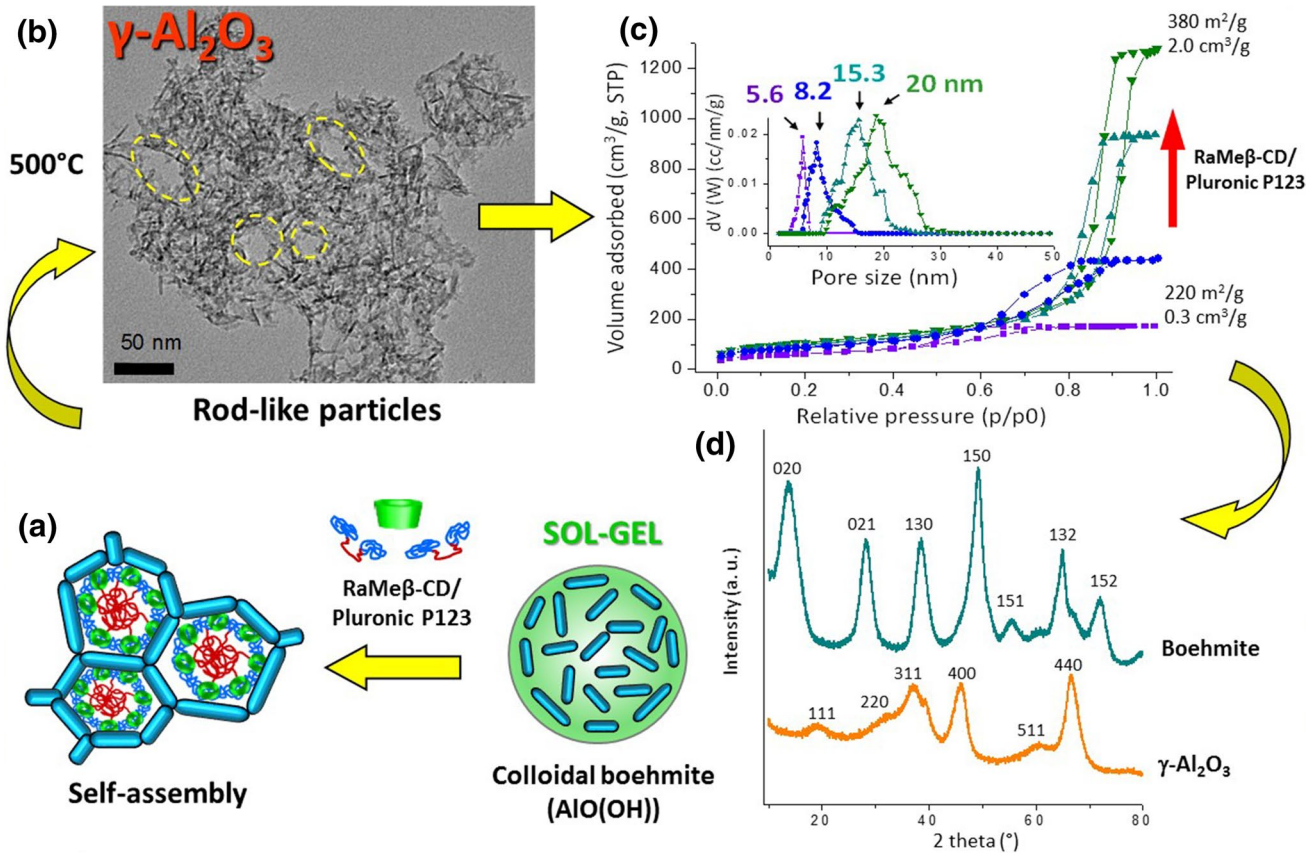

Fig. 9 **a** Schematic illustration of the template-directed synthesis of mesoporous γ-Al_2O_3 where boehmite (AlO(OH)) colloids act as building blocks for the construction of the hybrid organic-inorganic network. **b** Transmission electron microscopy (TEM) images for mesoporous γ-Al_2O_3 prepared with Randomly Methylated *β*-CD (RaMe*β*-CD)-loaded micelles (80 mg mL^{-1}). **c** N_2-adsorption isotherms and corresponding pore size distributions (inset) for the mesoporous γ-Al_2O_3 prepared without template, with Pluronic P123 (PEO/Al = 1) and with increasing amounts of RaMe*β*-CD (30–130 mg mL^{-1}). Note that the pore size can be tuned from 5.6 to 20 nm. **d** X-ray diffraction (XRD) patterns of boehmite dried at 60 °C and mesoporous γ-Al_2O_3 calcined at 500 °C. Adapted with permission from Bleta et al. (2013). Copyright 2013 American Chemical Society

Table 1 Textural characteristics of mesoporous γ-Al_2O_3 calcined at 500 °C

Sample	S_{BET} (m^2 g^{-1})	PV (cm^3 g^{-1})	S_{cum} (m^2 g^{-1})	V_{cum} (cm^3 g^{-1})	PS (nm)
Al-T500	219	0.28	227	0.26	5.6
P1-Al-T500	357	1.37	387	1.35	14.8
P1-CD30-Al-T500	354	1.45	387	1.43	14.9
P1-CD60-Al-T500	356	1.62	372	1.60	16.3
P1-CD80-Al-T500	382	1.97	427	1.94	19.3
P1-CD130-Al-T500	360	1.66	373	1.63	10.5 and 19.7

P [PEO]/[Al], *CD* RaMe*β*-CD concentration in the sol (mg mL^{-1}), *T* calcination temperature, S_{BET} BET specific surface area determined in the relative pressure range 0.1–0.25, *PV* pore volume calculated from adsorbed volume at $P/P_o = 0.995$, S_{cum}, V_{cum}, *PS* cumulative surface area, cumulative volume and pore size resulting from non-local density functional theory (NLDFT) calculations. Reprinted with permission from Bleta et al. (2013). Copyright 2013 American Chemical Society

P42/mnm). Bulk rutile is the only thermodynamically stable phase, while bulk anatase and bulk brookite are metastable (Zhang and Banfield 1998, 2000). Anatase has a band gap of 3.2 eV with the absorption edge at 386 nm which lies in the near UV range, whereas rutile has a lower band gap of 3.02 eV with the adsorption edge in the visible range at 416 nm. The anatase polymorph is usually reported to be more active than rutile (Pillai et al. 2007), mainly because of the fast electron–hole recombination in the latter which results from its lower band gap (Periyat et al. 2008).

We have investigated the effect of different cyclodextrins (natives and modified) on the properties of mesoporous TiO_2 materials prepared by the colloidal approach (Fig. 10a). Interestingly, from the representative field emission scanning electron microscopy (FE-SEM) images, it was noticed that the cyclodextrin had a strong impact on the morphology of titania catalysts. Therefore, compared to native β-CD which produced aggregated particles, RaMeβ-CD gave rise to a highly porous and interconnected network (Fig. 10b). A strong impact of the cyclodextrin was also noticed on the crystalline properties of these materials. Thus, before any thermal treatment, the sol–gel TiO_2 was composed of 68% anatase (A) (JCPDS card no. 00-021-1272) and 32% brookite (B) (JCPDS card no. 01-076-1934). The crystallite sizes determined from the Scherrer formula were 6.6 ± 0.8 nm (A) and 5.3 ± 0.6 nm (B). Such a small particle size was explained by the high hydrolysis ratio employed which favors fast nucleation rates producing small and well-crystallized nanoparticles. However, upon calcination at 500 °C, the small particles agglomerated and the increased degree of nanoparticle packing facilitated the phase transformation. Therefore, from the diffraction diagram of the control sol–gel TiO_2 (Fig. 10c), one can note the appearance of an intense sharp peak at $2\theta = 27.4°$ corresponding to the (110) plane of the rutile (R) (JCPDS card no. 00-034-0180), arising from the transformation of both anatase and brookite during calcination. The contents of anatase and brookite, determined from the Rietveld refinement, dropped to ~35 and ~27%, respectively, while ~38% rutile formed as a result of the sintering (Fig. 10d). Meanwhile, the size of these three polymorphs grew to 36 nm (A), 19 nm (B) and 60 nm (R) as the phase transformation progressed. Interestingly, when the cyclodextrin was utilized as structure directing agent, the rutile reflections remarkably decreased in intensity indicating a delay in the phase transformation (Fig. 10c). Interestingly, this phenomenon was more pronounced when RaMeβ-CD was used as structure directing agent. Thus, with RaMeβ-CD, the size of the crystallites decreased to 8-11 nm and the rutile content became negligible (less than 1%) with respect to the contents of anatase (~48%) and brookite (~52%).

The binding affinity of cyclodextrins on titania nanoparticles is highly dependent on their nature, natives or modified. In the case of the native α-CD, β-CD and γ-CD, the numerous hydroxyl groups, located on both the narrow and the wider ring faces, may favor the interaction of the macrocycle

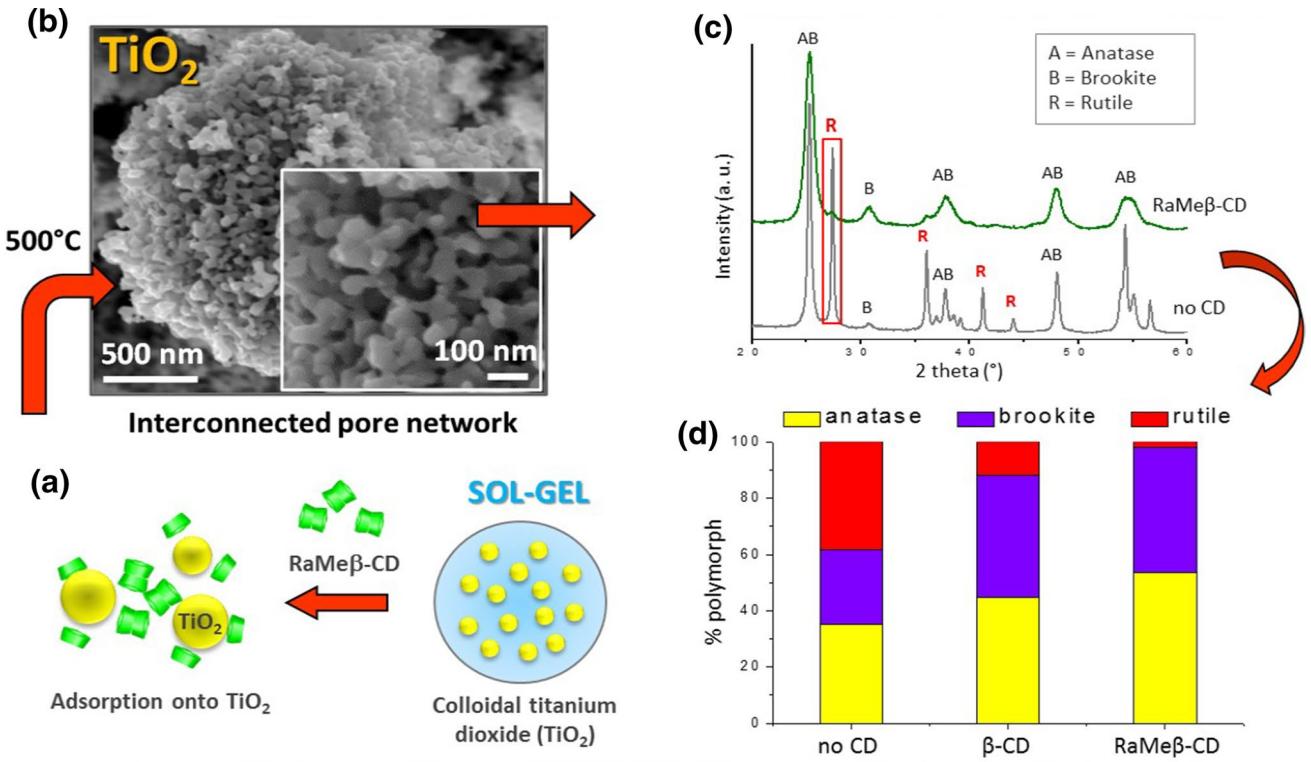

Fig. 10 **a** Schematic illustration of the self-assembly of TiO_2 colloids in the presence of the Randomly Methylated β-CD (RaMeβ-CD). **b** Representative field emission scanning electron micrographs (FE-SEM) of sol–gel TiO_2 prepared with RaMeβ-CD indicating the formation of highly interconnected pore network. **c** X-ray diffraction (XRD) patterns of the sol–gel TiO_2 prepared without CD and nanostructured TiO_2 prepared with RaMeβ-CD-based assemblies calcined at 500 °C. "A", "B" and "R" denote the anatase, brookite and rutile phases, respectively. **d** Crystal phase composition determined by XRD for the corresponding materials

with the surface –OH groups of TiO_2. Conversely, the 2-hydroxypropyl β-CD (HPβ-CD) and the randomly methylated β-CD (RaMeβ-CD), possessing less surface hydroxyl groups on the ring, are likely to form less hydrogen bonds. Additionally, the adsorption capacity of the modified cyclodextrins may be hindered by the steric constraint created by the 2-hydroxypropyl and methoxy groups, thus leaving less place for the interaction with the non-substituted hydroxyl groups.

The changes occurring in the structure of cyclodextrin assemblies after interaction with titania colloids and after solvent evaporation were followed by XRD measurements. From Fig. 11, it can be seen that the native α-CD and β-CD, before being introduced to the titania hydrosol, present several sharp diffraction lines characteristic of their cage-type crystalline microstructure (Harada et al. 2009). After interaction with titania colloids, the disappearance of the most intense reflections observed at 12.2°, 14.3° and 21.6° with the neat α-CD and at 9.0° and 12.5° with the neat β-CD suggested the disruption of the cage-type microstructure due to the adsorption of these oligosaccharides on the titania surface. On the other hand, the modified cyclodextrins (HPβ-CD and RaMeβ-CD) presented only two broad peaks due to their amorphous character. Interestingly, from the patterns of the hybrid HPβ-CD/TiO_2 and RaMeβ-CD/TiO_2 materials, it was noticed that these reflections were still intense, indicating weaker interactions with the titania surface.

The substitution of hydroxyl groups by a relatively large number of methoxy (–OCH_3) or 2-hydroxypropyl (–$OCH_2CH(CH_3)OH$) ones is one of the main factors that affects the physicochemical properties of the cyclodextrins, implying changes in both the solubility profile (due to the disruption of intermolecular hydrogen bonds) and the

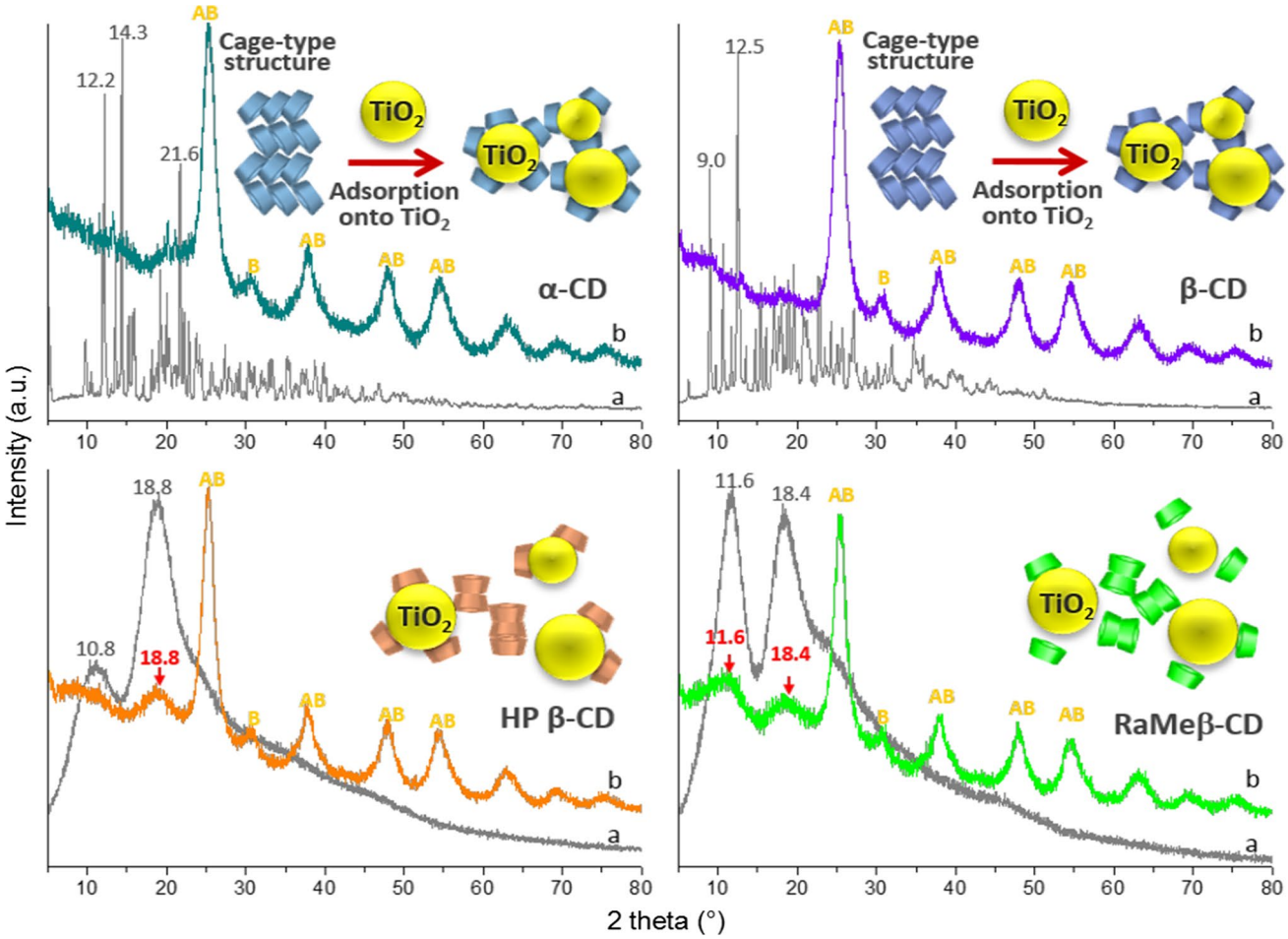

Fig. 11 X ray diffraction patterns of the neat cyclodextrins (**a**) and corresponding cyclodextrin (CD)/TiO_2 hybrid xerogels (**b**) prepared with a CD/Ti molar ratio of 0.076 for the native α-CD, the 2-HydroxyPropyl β-CD (HPβ-CD), and the Randomly Methylated β-CD (RaMeβ-CD) and 0.032 for the native β-CD. Xerogels were dried at 60 °C. Note that after interaction with TiO_2 colloids, the most intense reflections observed with the α-CD and β-CD disappear suggesting the disruption of the cage-type microstructure due to the adsorption of these cyclodextrins on the TiO_2 surface. Reprinted with permission from Bleta et al. (2014a) Copyright 2014 American Chemical Society

interfacial behavior (due to the presence of more marked hydrophobic and hydrophilic microenvironments). Thus, the surface tension data indicated that, in contrast to the native cyclodextrins, which are almost not surface-actives, HPβ-CD and RaMeβ-CD present surface tension values of 59.9 and 56.8 mN m^{-1}, respectively at 38 mM (concentration utilized for the preparation of the mesoporous titania materials). The slightly lower surface activity of HPβ-CD compared to RaMeβ-CD may be explained by the lower lipophilic character of the 2-hydroxypropyl groups compared to the methoxy ones. In this sense, the relatively higher surface activity of RaMeβ-CD may offer a means to reduce the surface energy of titania nanocrystals, thus facilitating their movement which is critical for their self-assembly. Significant modifications were also observed on the textural characteristics of the photocatalysts. Thus, using α-CD, the surface area increased from 21 to 68 m^2 g^{-1}, the pore volume from 0.03 to 0.13 cm^3 g^{-1} and the pore size from 5.3 to 7.0 nm. Similar results were also obtained with β-CD and γ-CD. Interestingly, the porosity was further enhanced when the modified cyclodextrins were used as structure directing agents and the most relevant textural characteristics were obtained for titania prepared with RaMeβ-CD presenting a specific surface are of 115 m^2 g^{-1}, a pore volume of 0.3 cm^3 g^{-1} and a pore size of 11.4 nm.

The overall picture emerging from these experimental data was that among the five cyclodextrins, the RaMeβ-CD presented the best combination of surface active properties and weak intermolecular interactions to efficiently direct the self-assembly of titania nanoparticles in a uniform network. The mechanism suggested for this self-assembly is dependent on the structure of each cyclodextrin. In the presence of the native cyclodextrins (α-CD, β-CD and γ-CD), the colloid interface is rather rough (due to its high surface energy) and the intermolecular interactions are strong (due to the numerous –OH groups), therefore the interactions between adsorbed cyclodextrins should favor the local agglomeration of titania nanoparticles during solvent evaporation, thus resulting in a less porous network. By contrast, in the presence of HPβ-CD and RaMeβ-CD, smoother interfaces are created by the lipophilic groups present in the macrocycle, leading to a decrease in the surface energy of titania nanocrystals and a reorganization of the colloids in a more homogeneous and porous network with small sizes and a fine morphology.

Some applications of cyclodextrin-derived TiO_2

Mesoporous UV-light responsive TiO_2 photocatalysts

It is today well-accepted that the photocatalytic reactions mainly take place on the surface of the irradiated semiconductor (Linsebigler et al. 1995). Consequently, in addition to the effect of the crystal phase composition mentioned above, other factors such as the crystallite size, the surface area, the pore volume, the orientation of the active faces and the adsorption properties of the pollutant are also likely to affect the photocatalytic activity (Ovenstone 2001; Yang et al. 2008; Chen and Caruso 2013; Nursam et al. 2015; Wang et al. 2013).

To evaluate the photocatalytic activity of the titania materials prepared using the different cyclodextrins as structure directing agents, phenoxyacetic acid (PAA), a toxic herbicide, was chosen as probe molecule for degradation under UV light (360 nm). PAA is a parent molecule of the well-known 2,4-dichlorophenoxyacetic acid (2,4-D) and 2,4,5-trichlorophenoxyacetic acid (2,4,5-T) herbicides (Singh et al. 2007). The PAA photodegradation rates obtained with the different photocatalysts after 7 h of exposure under UV-light illumination (360 nm) (Fig. 12) indicated the important role of cyclodextrins on the photocatalytic activity of titania. Thus, TiO_2 materials prepared from α-CD, β-CD and γ-CD were all photoactive under UV irradiation and gave a PAA degradation rate in the range of 58–64%, which was almost 45% higher than that of the sol–gel TiO_2 (43%). Further enhancement in the photocatalytic activity was noticed with the material prepared from HPβ-CD showing an intermediate PAA degradation rate of 72% between γ-CD (66%) and RaMeβ-CD (86%) (Fig. 12a). Moreover, the photocatalytic activity increased progressively upon addition of increasing amounts of RaMeβ-CD and a maximum degradation rate of 86% was reached for a RaMeβ-CD/Ti molar ratio of 0.076, which was twice that of the sol–gel TiO_2. Beyond this optimum, a gradual decrease in the photocatalytic activity to 77 and 68% was noticed.

The origin of the enhancement of the photocatalytic activity was related to a combined effect of improved textural characteristics and controlled crystalline properties. The high surface areas, which may be correlated with the small size of the crystallites (8–16 nm), should provide a large number of adsorption sites and active centers surrounding the electron–hole pairs, thus facilitating the first step of the photocatalytic reaction. On the other hand, the high pore volumes may allow for more PAA to be adsorbed on the internal surface of the pores, thus improving the diffusion of the substrate to the adsorption sites during the photocatalytic process. Finally, the low density of crystalline defects obtained for the material calcined at 500 °C may produce less grain boundaries and thus, a larger amount of charge carriers should reach the surface of the crystal to initiate the redox reactions.

Taken together, these results showed that the photocatalytic activity of TiO_2 materials may be correlated with their structural and textural characteristics, both of which depend on the concentration and chemical nature of the cyclodextrin employed. Indeed, the strongest effects in the pore volume,

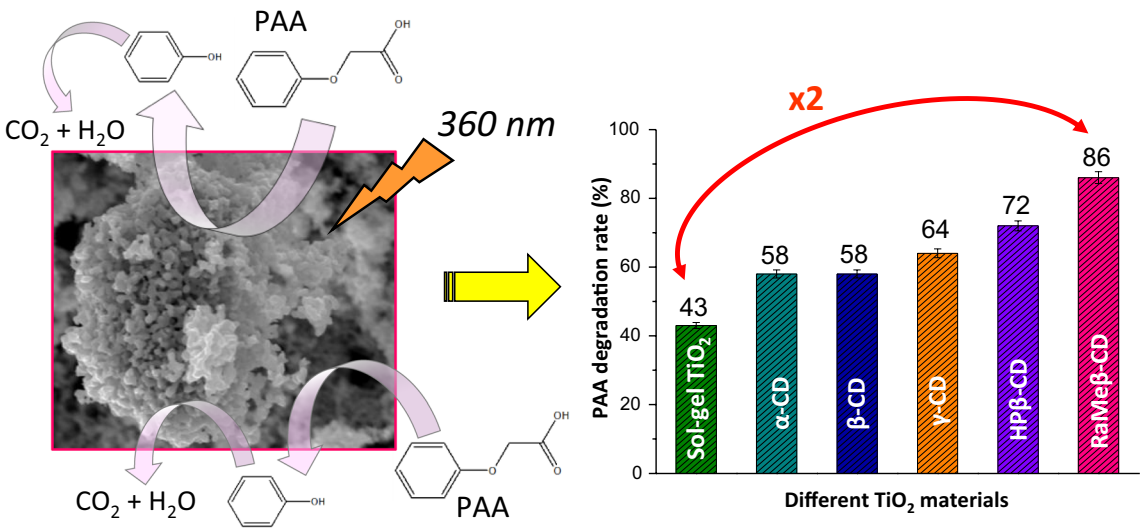

Fig. 12 Photodegradation rate of phenoxyacetic acid (PAA) after 7 h under UV-light irradiation on TiO_2 prepared with various cyclodextrins (CDs) at a fixed CD/Ti molar ratio: 0.076 for α-CD, γ-CD, 2-HydroxyPropyl β-CD (HPβ-CD), Randomly Methylated β-CD (RaMeβ-CD) and 0.032 for β-CD. Adapted with permission from Bleta et al. (2014a). Copyright 2014 American Chemical Society

surface area, phase composition and photocatalytic activity were observed when RaMeβ-CD was used as structure directing agent and for a calcination temperature of 500 °C. Overall, it was shown that all the above parameters are interlinked and a harmonization between them is necessary to obtain an efficient photocatalyst.

Mesoporous visible-light responsive Au/TiO_2 photocatalysts

In recent years, Au/TiO_2 composites have attracted much interest as efficient plasmonic photocatalysts owing to the ability of Au nanoparticles to absorb light in the visible region and TiO_2 to efficiently separate the photogenerated electrons and holes at the metal–semiconductor interface (Kowalska et al. 2009; Naya et al. 2014) (Wang et al. 2012; Wang and Caruso 2011). The redox ability of gold nanoparticles actually originates from their localized surface plasmon resonance (LSPR) arising from the collective oscillations of electrons on the nanoparticle surface under light irradiation (Lin et al. 2015) and depends both on particle size and shape (Park et al. 2007).

We have prepared highly active visible-light Au/TiO_2 photocatalysts by taking advantage of the ability of cyclodextrins to direct the self-assembly of TiO_2 colloids in a porous network over which Au nanoparticles can be uniformly dispersed (Lannoy et al. 2017). The photocatalysts were prepared by a one-pot synthesis approach by introducing the gold salt precursor (chloroauric acid, $HAuCl_4$) together with various cyclodextrins (α-CD, β-CD, γ-CD, RaMeβ-CD or HPβ-CD) in the TiO_2 sol prepared by sol–gel process (Bleta et al. 2010). After drying at 60 °C and calcination at 500 °C, a composite material made up of metallic Au nanoparticles (2.5 wt%) dispersed on the TiO_2 surface was recovered. In this approach, the cyclodextrin had a dual role, i.e., it acted as a structure directing agent to direct the self-assembly of TiO_2 colloids in a nanostructured network and, at the same time, it ensured uniform dispersion of gold nanoparticles over the mesoporous support (Fig. 13a).

Evidence for the key role of the cyclodextrins in the morphology of Au/TiO_2 composites was provided by electron microscopy. Both field emission scanning electron microscopy (FE-SEM) and transmission electron microscopy (TEM) observations confirmed the uniform dispersion of the particles over the porous support. Monomodal particles were formed with native β-CD, while RaMeβ-CD gave rise to bimodal particles (Fig. 13a). On the other hand, the natives α-CD and γ-CD presented a similar behavior to β-CD, giving rise to small monodisperse particles, while bigger and more polydisperse particles were formed with HPβ-CD.

Gold nanoparticles were clearly distinguished also in FE-SEM micrographs revealing intimate contact with the mesoporous TiO_2 support. Moreover, in contrast to β-CD which gave rise to dense and compact structures with sharp angular domains, over which small Au particles (~ 15–20 nm diameter) were uniformly dispersed (Fig. 14a, c), RaMeβ-CD exerted an opposing action, producing a highly porous framework over which two types of Au particles with average diameters of approximately 15–30 nm and 100–150 nm were formed (Fig. 14b, d).

Remarkably, all CD-derived photocatalysts presented enhanced photocatalytic performances compared with the corresponding sol–gel materials. RaMeβ-CD gave rise to the most efficient photocatalysts for the PAA degradation under both UV and visible-light irradiation. The reaction

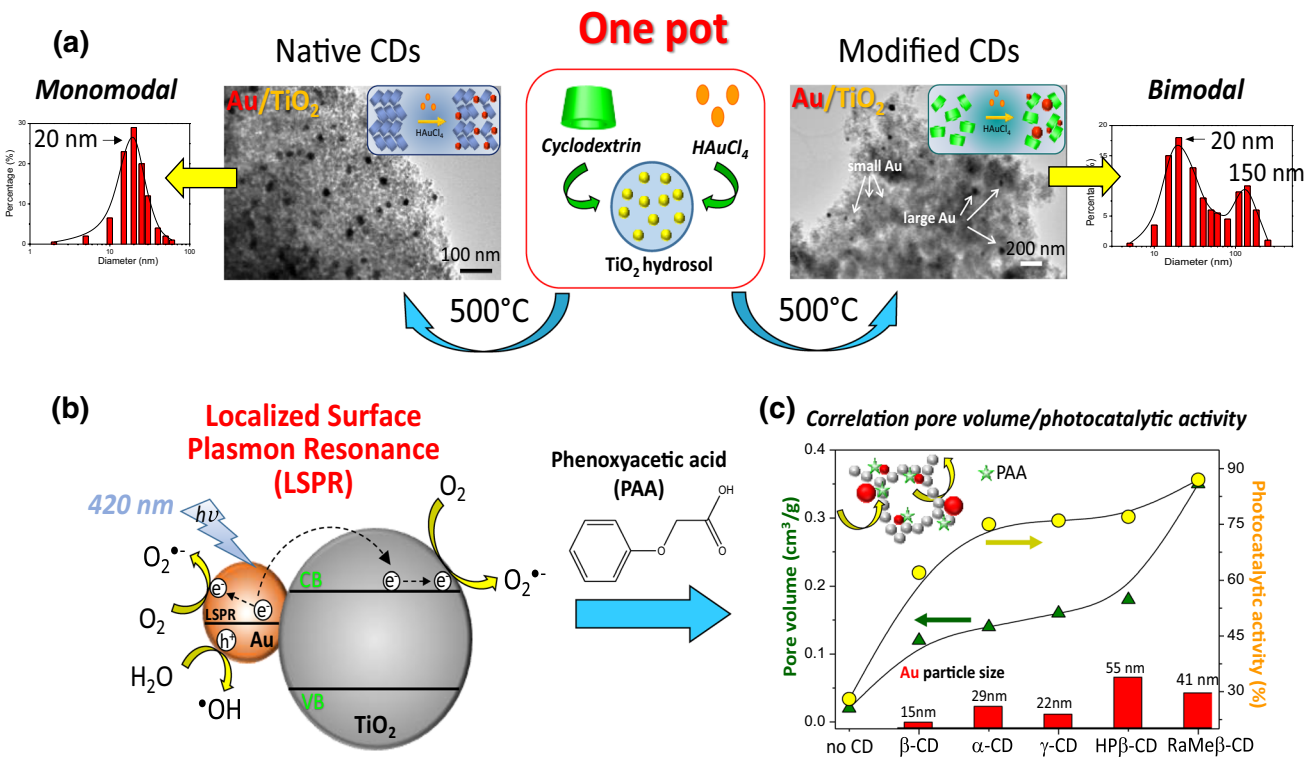

Fig. 13 **a** Transmission electron microscopy (TEM) bright-field images of the mesoporous Au/TiO_2 composites prepared by a one-pot synthesis using native and modified cyclodextrins as structure directing agents to direct the self-assembly of gold and TiO_2 colloids in a nanostructured framework. Note the formation of monomodal particles with native β-CD and bimodal particles with the Randomly Methylated β-CD (RaMe β-CD). **b** Visible-light-induced photocatalytic activity driven by localized surface plasmon resonance (LSPR) excitation of Au nanoparticles followed by interfacial electron transfer to the conduction band of TiO_2. **c** Effect of the pore volume and Au particle size on the activity of Au/TiO_2 composites in the photodegradation of phenoxyacetic acid (PAA) under visible-light irradiation (420 nm). Adapted with permission from Lannoy et al. (2017). Copyright 2017 American Chemical Society

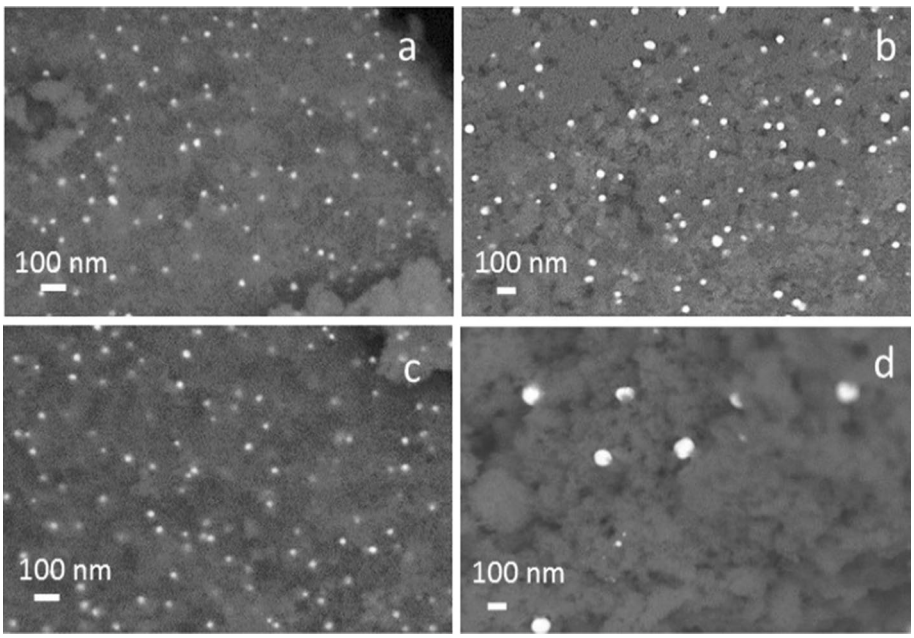

Fig. 14 Field emission scanning electron microscopy (FE-SEM) images recorded with back-scattered electrons on β-CD-derived Au/TiO_2 (**a**, **c**) and Randomly Methylated β-CD (RaMeβ-CD)-derived Au/TiO_2 composites (**b**, **d**). Adapted with permission from Lannoy et al. (2017). Copyright 2017 American Chemical Society

mechanism in these photocatalysts was different depending on whether excitation occurred on the semiconductor band gap (bare TiO_2) or on the surface plasmon of gold nanoparticles (Au-modified TiO_2). Thus, in the case of bare TiO_2 which is composed of anatase (Eg = 3.2 eV) and brookite (Eg = 3.3 eV), irradiation with UV-light is necessary to produce positive holes in the valence band (h^+_{VB}) and electrons in the conduction band (e^-_{CB}). The photogenerated holes can then oxidize adsorbed water and surface –OH groups (and eventually some PAA molecules), while the photogenerated electrons can reduce molecular oxygen adsorbed on the TiO_2 surface. These reactions can finally lead to the production of hydroxyl radicals ($^{\cdot}OH$) and superoxide radical anions ($O_2^{\cdot-}$), respectively, which are powerful oxidants for the degradation of organic pollutants in water. On the other hand, in the case of Au/TiO_2 composites (Fig. 13b), the electronic charge carriers responsible for the PAA degradation are likely to come mainly from the localized surface plasmon resonance (LSPR) excitation of gold nanoparticles under visible-light irradiation. Moreover, as the lifetime of electrons generated in the LSPR process is very short (less than 10^{-3} ns for Au nanoparticles), their intimate contact with the titania surface should favor the transfer of the hot electrons from the plasmonic Au nanoparticles to the TiO_2 conduction band, thus hindering the e^-/h^+ recombination and enhancing the photocatalytic efficiency (Clavero 2014).

On the basis of these results, it was concluded that the effect of cyclodextrins in increasing the porosity of both TiO_2 and Au/TiO_2 photocatalysts follows the order RaMeβ-CD > HPβ-CD > γ-CD ≈ α-CD > β-CD, while their effect in decreasing the size of gold nanoparticles follows an opposite trend, i.e., β-CD > γ-CD > α-CD > RaMeβ-CD > HPβ-CD (Fig. 13c). In addition to the porosity effect, the larger Au particles formed within the RaMeβ-CD-derived Au/TiO_2 photocatalysts are likely to improve the photoabsorption in a wider wavelength range, thus increasing the number of absorbed photons (Kowalska et al. 2009). In addition, the existence of gold particles with various dimensions within the same photocatalysts should also facilitate the electron transport from small to large particles through the conduction band of TiO_2 (Naya et al. 2014). Finally, the good crystallinity of both TiO_2 and Au particles may produce less defects and thus enhance the interfacial electron transfer rate between Au nanoparticles and the TiO_2 semiconductor.

Mesoporous RuO_2/TiO_2 composites with high catalytic performance in the hydrogenation of oils

In heterogeneous catalysis, the design of nanostructured support materials with high specific surface area and tailored porosity is of crucial importance for enhancing the catalyst effectiveness (Bell 2003; Alphonse et al. 2015). The approach combining the template-directed colloidal self-assembly with cyclodextrin-assisted impregnation method was also used to prepare highly active and selective Ru/TiO_2 catalysts for the hydrogenation of methyl oleate (MO, C18:1) to methyl stearate (MS, C18:0) under mild conditions (50 °C, 40 bar H_2) (Bleta et al. 2016). In a first step, the supramolecular assemblies formed between the block copolymer Pluronic P123 and RaMeβ-CD were used as template to prepare a highly porous TiO_2 support. Then, in a second step, Ru nanoparticles were dispersed over the support by impregnation, with or without the assistance of the native β-CD, to produce a RuO_2/TiO_2 composite (Fig. 15a). Before catalytic tests, RuO_2 was reduced in metallic Ru under H_2 flow at 400 °C for 4 h. Uniform dispersion of ruthenium nanoparticles was achieved over the large pores of RaMeβ-CD-P123-templated TiO_2 material.

To understand the effect of the CD-based assemblies, four RuO_2/TiO_2 composites (2.5 wt% Ru) were prepared using both conventional sol–gel TiO_2 prepared without cyclodextrins (containing ~ 35% anatase, ~ 26% brookite and ~ 39% rutile) and nanostructured RaMeβ-CD-P123-templated TiO_2 (containing ~ 48% anatase and ~ 52% brookite) as supports, without or with assistance of β-CD as dispersing agent. In addition to the diffraction lines of TiO_2, XRD patterns indicated also the presence of new reflexion lines at $2\theta = 27.8°$ and 34.9° which were indexed to the (110) and (101) planes, respectively, of the tetragonal RuO_2 (JCPDS 00-043-1027). For the TiO_2-sg supported catalysts, the (110) and (101) planes of RuO_2 and rutile-TiO_2 overlapped due to the lattice matching between these two phases both of which adopt a tetragonal structure. Moreover, it was shown that both the support and the dispersing agent could affect the size of RuO_2 crystallites. Thus, for the Ru2.5 and Ru2.5β-CD catalysts deposited over TiO_2-ns, the crystallite sizes determined from the line broadening of the (110) diffraction peak were 9.8 and 9.2 nm, respectively, while the average sizes obtained for the catalysts deposited over TiO_2-sg were beyond 10 nm.

Evidence for the key role of RaMeβ-CD-based assemblies on the dispersion of RuO_2 nanoparticles was provided by high-resolution transmission electron microscopy (HR-TEM) (Fig. 15b). Thus, the two phases, i.e., TiO_2 (white regions) and RuO_2 nanoparticles (dark regions) of the composite were clearly distinguished. TiO_2 nanoparticles contained tetragonal anatase (~ 15 nm) and orthorhombic brookite (~ 10 nm). Interestingly, mesopores of 15–20 nm diameter, resulting from the self-assembly of these nanoparticles around the supramolecular template, were also clearly visualized (pink circles), in agreement with N_2-adsorption analyses. On the other hand, RuO_2 nanoparticles were more or less spherical and approximately 10–12 nm in size, in agreement with XRD results. Conversely, the sol–gel catalyst prepared without cyclodextrin showed mainly a dense

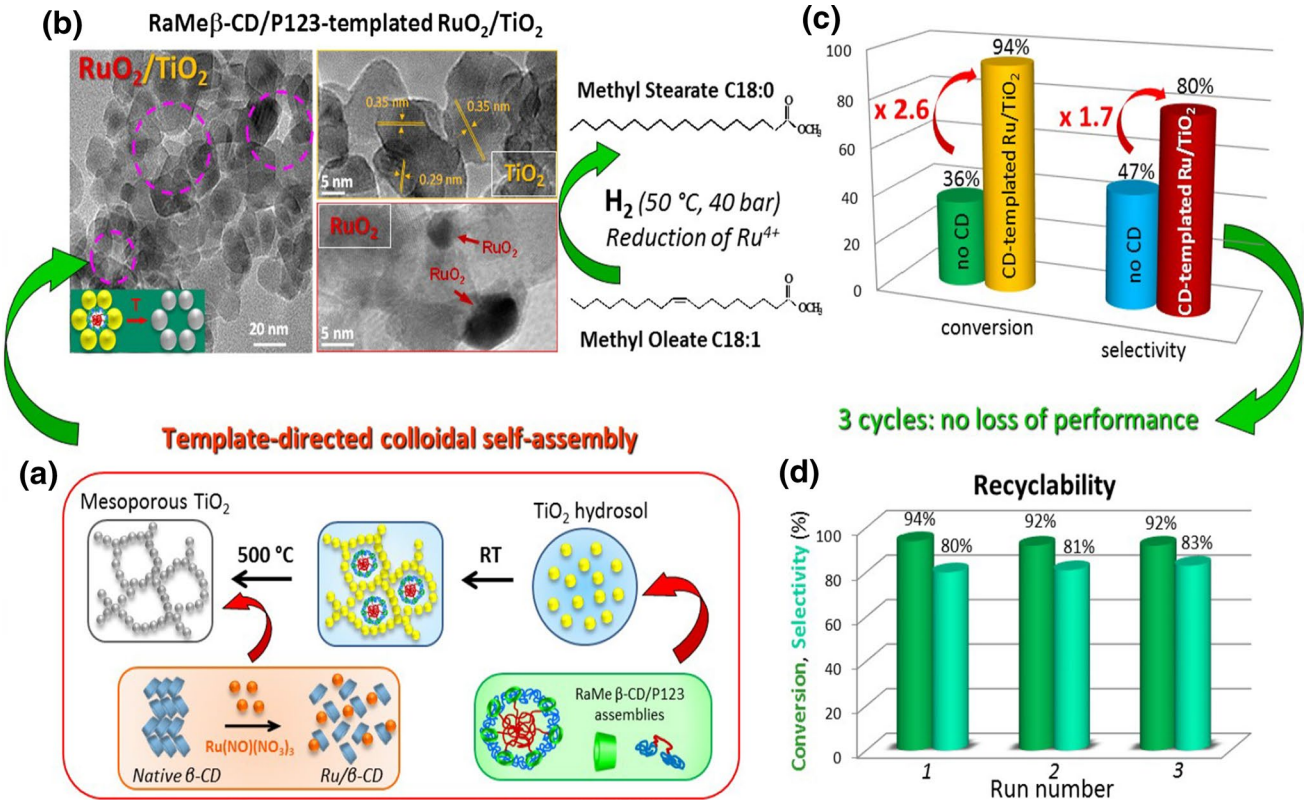

Fig. 15 **a** Schematic illustration of the synthesis of RuO_2/TiO_2 composites by template directed colloidal self-assembly (RaMeβ-CD: Randomly Methylated β-CD and P123: Pluronic $PEO_{20}PPO_{70}PEO_{20}$). Catalysts were calcined at 400 °C, then reduced under H_2 before being evaluated in the hydrogenation of methyl oleate (MO, C18:1) to methyl stearate (MS, C18:0). **b** High-resolution transmission electron micrographs of the RaMeβ-CD-P123-templated RuO_2/TiO_2 catalyst indicating uniform dispersion of anatase and brookite TiO_2 nanoparticles, as well as RuO_2 nanoparticles (5–10 nm). **c** Comparison of the conversion and selectivity of supported catalysts prepared with and without cyclodextrin. **d** Recyclability tests of the nanostructured catalyst. Adapted with permission of the Royal Society of Chemistry from Bleta et al. (2016)

network over which RuO_2 particles tended to form elongated heterogeneous structures. Such unusual epitaxial growth of RuO_2 nanoparticles over rutile-TiO_2 was also observed by Xiang et al. (2012) and was suggested to result from the structural matching between these two phases which actually share the same type of lattice symmetry (tetragonal) and have very similar lattice parameters (a = 4.59 Å, c = 2.96 Å for rutile-TiO_2 and a = 4.49 Å, c = 3.10 Å for RuO_2).

The performance of the different supported Ru/TiO_2 catalysts was evaluated in the liquid phase hydrogenation of methyl oleate (MO, C18:1) to methyl stearate (MS, C18:0) under mild conditions (40 bar H_2, 50 °C). Methyl esters of vegetable oils, derived from polyunsaturated fatty acids, can be transformed through partial or complete hydrogenation into saturated fatty acids with improved physical properties (e.g., high melting point and oxidative stability) (Philippaerts et al. 2013). Methyl stearate is an important saturated oil obtained from catalytic hydrogenation of unsaturated methyl oleate and widely used as a feedstock for catalytic hydrogenolysis into its corresponding saturated fatty alcohol (stearyl alcohol, C18:0) (Pritchard et al. 2015). Ru-based catalysts have been shown to be effective for low temperature hydrogenation of carboxylic acid esters, especially for selective hydrogenation of the olefinic C=C bond without affecting the carbonyl C=O bond.

Depending on the preparation method, the conversion and the selectivity were both affected (Fig. 15c). All supported Ru/TiO_2 catalysts were selective in the hydrogenation of the olefinic C=C bond producing the fully saturated ester, i.e., methyl stearate (C18:0) as the main product and the methyl elaïdate (C18:1, trans-9) as the only byproduct. In particular, the catalytic performance was strongly affected by the support prepared with or without cyclodextrin. Thus, when Ru was deposited over nanostructured RaMeβ-CD-P123-templated TiO_2, the methyl oleate conversion increased sharply from 36 to 94% using β-CD as dispersing agent which was almost threefold higher than that of Ru deposited over sol–gel TiO_2 prepared without the CD-based assemblies.

Similarly to the catalytic activity, clear differences were observed also in the selectivity toward methyl stearate which increased from 47 to 80% when the RaMeβ-CD-based assemblies were used as templates. However, here no beneficial effect was noticed when the β-CD was used as dispersing agent. The catalytic performance agreed well with the textural characteristics of the support and the degree of dispersion of the ruthenium species. Indeed, the highest performance of the RaMeβ-CD-P123 templated catalyst resulted from a combined effect of improved textural characteristics of the support and uniform dispersion of ruthenium nanoparticles. Thus, the high surface area of the RaMeβ-CD-P123 templated TiO_2 material (80 $m^2\ g^{-1}$) should provide a high level of dispersion of ruthenium nanoparticles, facilitating the contact of methyl oleate with the catalyst surface during the hydrogenation reaction. On the other hand, the high pore volume (0.36 $cm^3\ g^{-1}$) should allow for more reactant molecules to be adsorbed to the internal surface of the pores, thus improving the diffusion of reactants and products toward the active phase during the catalytic process. Finally, the use of native β-CD as dispersing agent may allow for reducing the interparticle aggregation thanks to the ability of this cyclodextrin to interact with both $RuNO(NO_3)_3$ and TiO_2 nanoparticles. Overall, these results revealed a dual role played by the CD-based assemblies, i.e., an enhancement of the porosity and surface area of the RuO_2/TiO_2 composites and a better dispersion of Ru nanoparticles over the support, parameters that appear to be essential for enhancing the efficacy of the catalyst in the liquid phase hydrogenation of methyl oleate.

Moreover, the recyclability of the most efficient catalyst, i.e., RaMeβ-CD-P123 templated TiO_2, was investigated in three successive runs. Remarkably, no loss of activity and selectivity was observed during the consecutive cycles, indicating high stability of the supported catalyst under the employed reaction conditions (Fig. 15d). The high surface area and large pore volume generated by the template-directed self-assembly of titania colloids should allow for a good dispersion of nanosized ruthenium particles and, therefore, effectively prevent aggregation while improving the chemical stability of the catalyst. Moreover, the thermal treatment at 400 °C should improve fixation of ruthenium species over the TiO_2 material, preventing leaching from the matrix to the reaction media during the catalytic process. The high efficacy of this catalyst combined with ease of recovery and reuse, without loss of conversion and selectivity, makes the colloidal self-assembly a simple and versatile approach for the synthesis of supported catalysts with high performance in liquid phase hydrogenation reactions.

Conclusion

In this review article, we have presented an overview of the different types of porous inorganic materials that can be prepared from cyclodextrins or cyclodextrin-based assemblies, ranging from microporous to mesoporous and further to hierarchically structured porous materials with a three-dimensional interconnected network. From the perspective of the synthesis, the approach that involves hydrolysis and catalytic polycondensation of a silicon alkoxide precursor around a supramolecular template is the most commonly used for the fabrication of silica materials. On the other hand, the template-directed colloidal self-assembly approach enables rational design of a broad range of non-siliceous materials with very high specific surface areas (380 $m^2\ g^{-1}$ for γ-Al_2O_3 and 110 $m^2\ g^{-1}$ for TiO_2), tailored porosities in the mesoscale (2–20 nm), controlled crystal phase compositions and various morphologies ranging from spheres, to rod-like particles and fibers. Moreover, metal nanoparticles (such as Ru, Au, Co, Mo) can also be uniformly dispersed within these materials providing nanostructured composites with tunable properties. With respect to catalytic applications, the cyclodextrin-derived porous materials and composites hold great promise owing to their unique structural and textural properties which are key factors in obtaining highly active, selective, stable and recyclable heterogeneous catalysts.

References

Alphonse P, Bleta R, Lavergne D, Barrault J, Maciuca A, Tatibouët JM, Rossignol C (2015) Patent No. WO 2015/055672 A1

Antonietti M (2006) Silica nanocasting of lyotropic surfactant phases and organized organic matter: material science or an analytical tool? Philos Trans R Soc A 364:2817–2840. https://doi.org/10.1098/rsta.2006.1857

Armbrust EV (2009) The life of diatoms in the world's oceans. Nature 459:185–192. https://doi.org/10.1038/nature08057

Armbrust E, Berges J, Bowler C, Green B, Martinez D, Putnam N, Rokhsar D (2004) The genome of the diatom Thalassiosira pseudonana: ecology, evolution, and metabolism. Science 306:79–86. https://doi.org/10.1126/science.1101156

Beck J, Vartuli J, Roth W, Leonowicz M, Kresge C, Schmitt K, Schlenker JL (1992) A new family of mesoporous molecular sieves prepared with liquid crystal templates. J Am Chem Soc 114:10834–10843. https://doi.org/10.1021/ja00053a020

Bell A (2003) The impact of nanoscience on heterogeneous catalysis. Science 299:1688–1691. https://doi.org/10.1126/science.1083671

Bernat V, Ringard-Lefebvre C, Bas G, Perly B, Djedaïni-Pilard F, Lesieur S (2008) Inclusion complex of n-octyl β-d-glucopyranoside and α-cyclodextrin in aqueous solutions: thermodynamic and structural characterization. Langmuir 24:3140–3149. https://doi.org/10.1021/la7034906

Bleta R, Blin J, Stebe M (2006) Solubilization of various fluorocarbons in a fluorinated surfactant/water system: relation with the

design of porous materials. J Phys Chem B 110:23547–23556. https://doi.org/10.1021/jp0644199

Bleta R, Alphonse P, Lorenzato L (2010) Nanoparticle route for the preparation in aqueous medium of mesoporous TiO2 with controlled porosity and crystalline framework. J Phys Chem C 114:2039–2048. https://doi.org/10.1021/jp909646h

Bleta R, Jaubert O, Gressier M, Menu M (2011) Rheological behaviour and spectroscopic investigations of cerium-modified AlO(OH) colloidal suspensions. J Colloid Interface Sci 363:557–565. https://doi.org/10.1016/j.jcis.2011.08.008

Bleta R, Alphonse P, Pin L, Gressier M, Menu M (2012) An efficient route to aqueous phase synthesis of nanocrystalline γ-Al2O3 with high porosity: from stable boehmite colloids to large pore mesoporous alumina. J Colloid Interface Sci 367:120–128. https://doi.org/10.1016/j.jcis.2011.08.087

Bleta R, Machut C, Leger B, Monflier E, Ponchel A (2013) Coassembly of block copolymer and randomly methylated β-cyclodextrin: from swollen micelles to mesoporous alumina with tunable pore size. Macromolecules 46:5672–5683. https://doi.org/10.1021/ma4008303

Bleta R, Lannoy A, Machut C, Monflier E, Ponchel A (2014a) Understanding the role of cyclodextrins in the self-assembly, crystallinity, and porosity of titania nanostructures. Langmuir 30:11812–11822. https://doi.org/10.1021/la502911v

Bleta R, Machut C, Leger B, Monflier E, Ponchel A (2014b) Investigating the effect of randomly methylated β-cyclodextrin/block copolymer molar ratio on the template-directed preparation of mesoporous alumina with tailored porosity. J Incl Phenom Macrocycl Chem 80:323–335. https://doi.org/10.1007/s10847-014-0405-7

Bleta R, Menuel S, Leger B, Da Costa A, Monflier E, Ponchel A (2014c) Evidence for the existence of crosslinked crystalline domains within cyclodextrin-based supramolecular hydrogels through sol-gel replication. RSC Adv 4:8200–8208. https://doi.org/10.1039/C3RA47765G

Bleta R, Noel S, Addad A, Ponchel A, Monflier E (2016) Mesoporous RuO2/TiO2 composites prepared by cyclodextrin-assisted colloidal self-assembly: towards efficient catalysts for the hydrogenation of methyl oleate. RSC Adv 6:14570–14579. https://doi.org/10.1039/C5RA27161D

Bleta R, Monflier E, Ponchel A (2018) Cyclodextrins and nanostructured porous inorganic materials. In: Fourmentin S, Crini G, Lichtfouse E (eds) Cyclodextrin fundamentals, reactivity and analysis (Series: Environmental Chemistry for a Sustainable World). Springer. ISBN: 978-3-319-76158-9. https://doi.org/10.1007/978-3-319-76159-6_3

Bleta R, Schiavo B, Corsaro N, Costa P, Giaconia A, Interrante L, Galia A (2018b) Robust mesoporous CoMo/γ-Al2O3 catalysts from cyclodextrin-based supramolecular assemblies for hydrothermal processing of microalgae: effect of the preparation method. ACS Appl Mater Interfaces 10:12562–12579. https://doi.org/10.1021/acsami.7b16185

Blin J, Bleta R, Ghanbaja J, Stebe M (2006) Fluorinated emulsions: templates for the direct preparation of macroporous-mesoporous silica with a highly ordered array of large mesopores. Microporous Mesoporous Mater 94:74–80. https://doi.org/10.1016/j.micromeso.2006.03.023

Boal A, Ilhan F, DeRouchey J, Thurn-Albrecht T, Russell T, Rotello V (2000) Self-assembly of nanoparticles into structured spherical and network aggregates. Nature 404:746–748. https://doi.org/10.1038/35008037

Born M, Ritter H (1995) Side-chain polyrotaxanes with a tandem structure based on cyclodextrins and a polymethacrylate main chain. Angew Chem Int Ed Engl 34:309–311. https://doi.org/10.1002/anie.199503091

Breslow R, Dong S (1998) Biomimetic reactions catalyzed by cyclodextrins and their derivatives. Chem Rev 98:1997–2011. https://doi.org/10.1021/cr970011j

Chen D, Caruso R (2013) Recent progress in the synthesis of spherical titania nanostructures and their applications. Adv Funct Mater 23:1356–1374. https://doi.org/10.1002/adfm.201201880

Clavero C (2014) Plasmon-induced hot-electron generation at nanoparticle/metal-oxide interfaces for photovoltaic and photocatalytic devices. Nat Photonics 8:95–103. https://doi.org/10.1038/nphoton.2013.238

Corma A (1997) From microporous to mesoporous molecular sieve materials and their use in catalysis. Chem Rev 97:2373–2420. https://doi.org/10.1021/cr960406n

Corma A, Moliner M, Diaz-Cabanas MJ, Serna P, Femenia B, Primo J, Garcia H (2008) Biomimetic synthesis of microporous and mesoporous materials at room temperature and neutral pH, with application in electronics, controlled release of chemicals, and catalysis. New J Chem 32:1338–1345. https://doi.org/10.1039/B808697B

Davis M (2002) Ordered porous materials for emerging applications. Nature 417:813–821. https://doi.org/10.1038/nature00785

Dreiss C, Nwabunwann E, Liu R, Brooks N (2009) Assembling and de-assembling micelles: competitive interactions of cyclodextrins and drugs with Pluronics. Soft Matter 5:1888–1896. https://doi.org/10.1039/B812805G

Fujishima A, Honda K (1972) Electrochemical photolysis of water at a semiconductor electrode. Nature 238:37–38. https://doi.org/10.1038/238037a0

Gaitano G, Brown W, Tardajos G (1997) Inclusion complexes between cyclodextrins and triblock copolymers in aqueous solution: a dynamic and static light-scattering study. J Phys Chem B 101:710–719. https://doi.org/10.1021/jp961996w

Gomathi Devi L, Kavitha R (2013) A review on non-metal ion doped titania for the photocatalytic degradation of organic pollutants under UV/solar light: role of photogenerated charge carrier dynamics in enhancing the activity. Appl Catal B 140–141:559–587. https://doi.org/10.1016/j.apcatb.2013.04.035

Hamm CE, Merkel R, Springer O, Jurkojc P, Maier C, Prechtel K, Smetacek V (2003) Architecture and material properties of diatom shells provide effective mechanical protection. Nature 421:841–843. https://doi.org/10.1038/nature01416

Han BH, Antonietti M (2002) Cyclodextrin-based pseudopolyrotaxanes as templates for the generation of porous silica materials. Chem Mater 14:3477–3485. https://doi.org/10.1021/cm0113088

Han BH, Smarsly B, Gruber C, Wenz G (2003) Towards porous silica materials via nanocasting of stable pseudopolyrotaxanes from α-cyclodextrin and polyamines. Microporous Mesoporous Mater 66:127–132. https://doi.org/10.1016/j.micromeso.2003.09.003

Hao E, Lian T (2000) Layer-by-layer assembly of CdSe nanoparticles based on hydrogen bonding. Langmuir 16:7879–7881. https://doi.org/10.1021/la000761f

Harada A (1996) Preparation and structures of supramolecules between cyclodextrins and polymers. Coord Chem Rev 148:115–133. https://doi.org/10.1016/0010-8545(95)01157-9

Harada A (2001) Cyclodextrin-based molecular machines. Acc Chem Res 34:456–464. https://doi.org/10.1021/ar000174l

Harada A, Kamachi M (1990) Complex formation between poly (ethylene glycol) and α-cyclodextrin. Macromolecules 23:2821–2823. https://doi.org/10.1021/ma00212a039

Harada A, Hashidzume A, Yamaguchi H, Takashima Y (2009) Polymeric rotaxanes. Chem Rev 109:5974–6023. https://doi.org/10.1021/cr9000622

Herrmann W, Keller W, Wenz G (1997) Kinetics and thermodynamics of the inclusion of ionene-6, 10 in α-cyclodextrin in an aqueous solution. Macromolecules 30:4966–4972. https://doi.org/10.1021/ma961373g

Hildebrand M (2008) Diatoms, biomineralization processes, and genomics. Chem Rev 108:4855–4874. https://doi.org/10.1021/cr078253z

Holmqvist P, Alexandridis P, Lindman B (1998) Modification of the microstructure in block copolymer-water-"oil" systems by varying the copolymer composition and the "oil" type: small-angle X-ray scattering and deuterium-NMR investigation. J Phys Chem B 102:1149–1158. https://doi.org/10.1021/jp9730297

Imhof A, Pine D (1997) Ordered macroporous materials by emulsion templating. Nature 389:948–951. https://doi.org/10.1038/40105

Jiang B, Guo D, Liu Y (2010) Self-assembly of amphiphilic perylene-cyclodextrin conjugate and vapor sensing for organic amines. J Org Chem 75:7258–7264. https://doi.org/10.1021/jo1014596

Joseph J, Dreiss C, Cosgrove T, Pedersen J (2007) Rupturing polymeric micelles with cyclodextrins. Langmuir 23:460–466. https://doi.org/10.1021/la061850g

Kooistra W, Gersonde R, Medlin L, Mann D (2007) The origin and evolution of diatoms: their adaptation to a planktonic existence. In: Falkowski PG, Knoll AH (eds) Evolution of primary producers in the sea. Elsevier, Boston, pp 207–249. https://doi.org/10.1016/B978-012370518-1/50012-6

Kowalska E, Abe R, Ohtani B (2009) Visible light-induced photocatalytic reaction of gold-modified titanium(IV) oxide particles: action spectrum analysis. Chem Commun. https://doi.org/10.1039/B815679D

Kresge CT, Leonowicz ME, Roth WJ, Vartuli JC, Beck JS (1992) Ordered mesoporous molecular sieves synthesized by a liquid-crystal template mechanism. Nature 359:710–712. https://doi.org/10.1038/359710a0

Kröger N, Poulsen N (2008) Diatoms from cell wall biogenesis to nanotechnology. Annu Rev Genet 42:83–107. https://doi.org/10.1146/annurev.genet.41.110306.130109

Kröger N, Deutzmann R, Sumper M (1999) Polycationic peptides from diatom biosilica that direct silica nanosphere formation. Science 286:1129–1132. https://doi.org/10.1126/science.286.5442.1129

Lannoy A, Bleta R, Machut C, Monflier E, Ponchel A (2014) Block copolymer-cyclodextrin supramolecular assemblies as soft templates for the synthesis of titania materials with controlled crystallinity, porosity and photocatalytic activity. RSC Adv 4:40061–40070. https://doi.org/10.1039/C4RA05994H

Lannoy A, Bleta R, Machut-Binkowski C, Addad A, Monflier E, Ponchel A (2017) Cyclodextrin-directed synthesis of gold-modified TiO2 materials and evaluation of their photocatalytic activity in the removal of a pesticide from water: effect of porosity and particle size. ACS Sustain Chem Eng 5:3623–3630. https://doi.org/10.1021/acssuschemeng.6b03059

Lazzara G, Milioto S (2008) Copolymer-cyclodextrin inclusion complexes in water and in the solid state. A physico-chemical study. J Phys Chem B 112:11887–11895. https://doi.org/10.1021/jp8034924

Leclercq L, Bricout H, Tilloy S, Monflier E (2007) Biphasic aqueous organometallic catalysis promoted by cyclodextrins: can surface tension measurements explain the efficiency of chemically modified cyclodextrins? J Colloid Interface Sci 307:481–487. https://doi.org/10.1016/j.jcis.2006.12.001

Li J, Harada A, Kamashi M (1994) Sol-gel transition during inclusion complex formation between α-cyclodextrin and high molecular weight poly(ethylene glycol)s in aqueous solution. Polym J 26:1019–1026. https://doi.org/10.1295/polymj.26.1019

Lin Z, Wang X, Liu J, Tian Z, Dai L, He B, Hu Z (2015) On the role of localized surface plasmon resonance in UV–Vis light irradiated Au/TiO2 photocatalysis systems: pros and cons. Nanoscale 7:4114–4123. https://doi.org/10.1039/C4NR06929C

Linsebigler A, Lu G, Yates J (1995) Photocatalysis on TiO2 surfaces: principles, mechanisms, and selected results. Chem Rev 95:735–758. https://doi.org/10.1021/cr00035a013

Liu Y, Goebl J, Yin Y (2013) Templated synthesis of nanostructured materials. Chem Soc Rev 42:2610–2653. https://doi.org/10.1039/C2CS35369E

Lu AH, Schüth F (2006) Nanocasting: a versatile strategy for creating nanostructured porous materials. Adv Mater 18:1793–1805. https://doi.org/10.1002/adma.200600148

Lu C, Wu N, Jiao X, Luo C, Cao W (2003) Micropatterns constructed from Au nanoparticles. Chem Commun. https://doi.org/10.1039/B301059G

Mahata A, Bose D, Ghosh D, Jana B, Bhattacharya B, Sarkar D, Chattopadhyay N (2010) Studies of Triton X-165-β-cyclodextrin interactions using both extrinsic and intrinsic fluorescence. J Colloid Interface Sci 347:252–259. https://doi.org/10.1016/j.jcis.2010.03.048

Misra C (1986) Industrial alumina chemicals. Washington, DC: Am. Chem. Soc. Collection ACS Monograph 184

Naya S, Niwa T, Kume T, Tada H (2014) Visible-light-induced electron transport from small to large nanoparticles in bimodal gold nanoparticle-loaded titanium(IV) oxide. Angew Chem 126:7433–7437. https://doi.org/10.1002/anie.201402939

Nogueiras-Nieto L, Alvarez-Lorenzo C, Sandez-Macho I, Concheiro A, Otero-Espinar F (2009) Hydrosoluble cyclodextrin/poloxamer polypseudorotaxanes at the air/water interface, in bulk solution, and in the gel state. J Phys Chem B 113:2773–2782. https://doi.org/10.1021/jp809806w

Nursam N, Wang X, Caruso R (2015) Macro-/mesoporous titania thin films: analysing the effect of pore architecture on photocatalytic activity using high-throughput screening. J Mater Chem A 3:24557–24567. https://doi.org/10.1039/C5TA08959J

Ovenstone J (2001) Preparation of novel titania photocatalysts with high activity. J Mater Sci 36:1325–1329. https://doi.org/10.1023/A:1017587016915

Park J, Momma T, Osaka T (2007) Spectroelectrochemical phenomena on surface plasmon resonance of Au nanoparticles immobilized on transparent electrode. Electrochim Acta 52:5914–5923. https://doi.org/10.1016/j.electacta.2007.03.029

Patolsky F, Weizmann Y, Lioubashevski O, Willner I (2002) Au-nanoparticle nanowires based on DNA and polylysine templates. Angew Chem Int Ed 41:2323–2327. https://doi.org/10.1002/1521-3757(20020703)114:13<2429:AID-ANGE2429>3.0.CO;2-G

Periyat P, Pillai S, McCormack D, Colreavy J, Hinder S (2008) Improved high-temperature stability and sun-light-driven photocatalytic activity of sulfur-doped anatase TiO2. J Phys Chem C 112:7644–7652. https://doi.org/10.1021/jp0774847

Philippaerts A, Jacobs P, Sels B (2013) Is there still a future for hydrogenated vegetable oils? Angew Chem Int Ed 52:5220–5226. https://doi.org/10.1002/anie.201209731

Pillai S, Periyat P, George R, Colreavy J, George R, Hayden H, Hinder S (2007) Synthesis of high-temperature stable anatase TiO2 photocatalyst. J Phys Chem C 111:1605–1611. https://doi.org/10.1021/jp065933h

Polarz S, Antonietti M (2002) Porous materials via nanocasting procedures: innovative materials and learning about soft-matter organization. Chem Commun. https://doi.org/10.1039/B205708P

Polarz S, Smarsly B, Bronstein L, Antonietti M (2001) From cyclodextrin assemblies to porous materials by silica templating. Angew Chem Int Ed 40:4417–4421. https://doi.org/10.1002/1521-3773(20011203)40:23<4417:AID-ANIE4417>3.0.CO;2-P

Pritchard J, Filonenko G, van Putten R, Hensen E, Pidko E (2015) Heterogeneous and homogeneous catalysis for the hydrogenation of carboxylic acid derivatives: history, advances and future directions. Chem Soc Rev 44:3808–3833. https://doi.org/10.1039/C5CS00038F

Rajh T, Micic O, Nozik A (1993) Synthesis and characterization of surface-modified colloidal CdTe qunatum dots. J Phys Chem 97:11999–12003. https://doi.org/10.1021/j100148a026

Saenger W (1980) Cyclodextrin inclusion compounds in research and industry. Angew Chem Int Ed Engl 19:344–362. https://doi.org/10.1002/anie.198003441

Singh H, Saquib M, Haque M, Muneer M, Bahnemann D (2007) Titanium dioxide mediated photocatalysed degradation of phenoxyacetic acid and 2,4,5-trichlorophenoxyacetic acid in aqueous suspensions. J Mol Catal A Chem 264:66–72. https://doi.org/10.1016/j.molcata.2006.08.088

Su BL, Sanchez C, Yang XE (2012) Hierarchically structured porous materials. From nanoscience to catalysis, separation, optics, energy, and life science. Wiley, Weinheim

Sumper M, Hett R, Lehmann G, Wenzl S (2007) A code for lysine modifications of a silica biomineralizing silaffin protein. Angew Chem Int Ed 46:8405–8408. https://doi.org/10.1002/ange.200702413

Sun M, Huang S, Chen L, Li Y, Yang X, Yuan Z, Su B (2016) Applications of hierarchically structured porous materials from energy storage and conversion, catalysis, photocatalysis, adsorption, separation, and sensing to biomedicine. Chem Soc Rev 45:3479–3563. https://doi.org/10.1039/C6CS00135A

Szejtli J (1998) Introduction and general overview of cyclodextrin chemistry. Chem Rev 98:1743–1753. https://doi.org/10.1021/cr970022c

Travelet C, Schlatter G, Hebraud P, Brochon C, Lapp A, Anokhin D, Hadziioannou G (2008) Multiblock copolymer behaviour of α-CD/PEO-based polyrotaxanes: towards nano-cylinder self-organization of α-CDs. Soft Matter 4:1855–1860. https://doi.org/10.1039/B806656F

Travelet C, Schlatter G, Hebraud P, Brochon C, Lapp A, Hadziioannou G (2009) Formation and self-organization kinetics of α-CD/PEO-based pseudo-polyrotaxanes in water. A specific behavior at 30 °C. Langmuir 25:8723–8734. https://doi.org/10.1021/la900070v

Travelet C, Hebraud P, Perry C, Brochon C, Hadziioannou G, Lapp A, Schlatter G (2010) Temperature-dependent structure of α-CD/PEO-based polyrotaxanes in concentrated solution in DMSO: kinetics and multiblock copolymer behavior. Macromolecules 43:1915–1921. https://doi.org/10.1021/ma902686p

Tsai C, Zhang W, Wang C, Van Horn R, Graham M, Huang J, Cheng S (2010) Evidence of formation of site-selective inclusion complexation between β-cyclodextrin and poly(ethylene oxide)-block-poly(propylene oxide)-block poly(ethylene oxide) copolymers. J Chem Phys 132:1–9. https://doi.org/10.1063/1.3428769

Uekama K, Irie T (1987) Pharmaceutical applications of methylated cyclodextrin derivatives. In: Duchêne D (ed) Cyclodextrins and their industrial uses. Editions de la Santé, Paris, pp 395–439

Valero M, Grillo I, Dreiss C (2012) Rupture of Pluronic micelles by dimethylated β-cyclodextrin is not due to polypseudorotaxane formation. J Phys Chem B 116:1273–1281. https://doi.org/10.1021/jp210439n

Van Der Voort P, Vercaemst C, Schaubroeck D, Verpoort F (2008) Ordered mesoporous materials at the beginning of the third millennium: new strategies to create hybrid and non-siliceous variants. Phys Chem Chem Phys 10:347–360. https://doi.org/10.1039/B707388G

Velev O, Kaler E (2000) Structured porous materials via colloidal crystal templating: from inorganic oxides to metals. Adv Mater 7:531–534. https://doi.org/10.1002/(SICI)1521-4095(200004)12:7<531:AID-ADMA531>3.0.CO;2-S

Walcarius A (2013) Mesoporous materials and electrochemistry. Chem Soc Rev 42:4098–4140. https://doi.org/10.1039/C2CS35322A

Wan Y, Zhao D (2007) On the controllable soft-templating approach to mesoporous silicates. Chem Rev 107:2821–2859. https://doi.org/10.1021/cr068020s

Wang X, Caruso R (2011) Enhancing photocatalytic activity of titania materials by using porous structures and the addition of gold nanoparticles. J Mater Chem 21:20–28. https://doi.org/10.1039/C0JM02620D

Wang X, Blackford M, Prince K, Caruso RA (2012) Preparation of boron-doped porous titania networks containing gold nanoparticles with enhanced visible-light photocatalytic activity. ACS Appl Mater Interfaces 4:476–482. https://doi.org/10.1021/am201695c

Wang X, Cao L, Chen D, Caruso R (2013) Engineering of monodisperse mesoporous titania beads for photocatalytic applications. ACS Appl Mater Interfaces 5:9421–9428. https://doi.org/10.1021/am401867s

Weickenmeier M, Wenz G (1997) Threading of cyclodextrins onto a polyester of octanedicarboxylic acid and polyethylene glycol. Macromol Rapid Commun 18:1109–1115. https://doi.org/10.1002/marc.1997.030181215

Wenz G (1994) Cyclodextrins as building blocks for supramolecular structures and functional units. Angew Chem Int Ed Engl 33:803–822. https://doi.org/10.1002/anie.199408031

Xiang G, Shi X, Wu Y, Zhuang J, Wang X (2012) Size effects in atomic-level epitaxial redistribution process of RuO2 over TiO2. Sci Rep 2(801):1–6. https://doi.org/10.1038/srep00801

Yang H, Sun C, Qiao S, Zou J, Liu G, Smith S, Lu G (2008) Anatase TiO2 single crystals with a large percentage of reactive facets. Nature 453:638–641. https://doi.org/10.1038/nature06964

Yang X, Chen L, Li Y, Rooke J, Sanchez C, Su B (2017) Hierarchically porous materials: synthesis strategies and structure design. Chem Soc Rev 46:481–558. https://doi.org/10.1039/C6CS00829A

Yu W, Peng X (2002) Formation of high-quality CdS and other II–VI semiconductor nanocrystals in noncoordinating solvents: tunable reactivity of monomers. Angew Chem Int Ed 41:2368–2371. https://doi.org/10.1002/1521-3773(20020703)41:13<2368:AID-ANIE2368>3.0.CO;2-G

Zhang H, Banfield J (1998) Thermodynamic analysis of phase stability of nanocrystalline titania. J Mater Chem 8:2073–2076. https://doi.org/10.1039/A802619J

Zhang H, Banfield J (2000) Understanding polymorphic phase transformation behavior during growth of nanocrystalline aggregates: insights from TiO2. J Phys Chem B 104:3481–3487. https://doi.org/10.1021/jp000499j

Zhao W, Ma W, Chen C, Zhao J, Shuai Z (2004) Efficient degradation of toxic organic pollutants with Ni_2O_3/TiO_{2-x} Bx under visible irradiation. J Am Chem Soc 126:4782–4783. https://doi.org/10.1021/ja0396753

Zhu C, Du D, Eychmüller A, Lin Y (2015) Engineering ordered and nonordered porous noble metal nanostructures: synthesis, assembly, and their applications in electrochemistry. Chem Rev 115:8896–8943. https://doi.org/10.1021/acs.chemrev.5b00255